The Evolution of the Solar-Stellar Activity

Maria M. Katsova

Sternberg State Astronomical Institute

Moscow State University

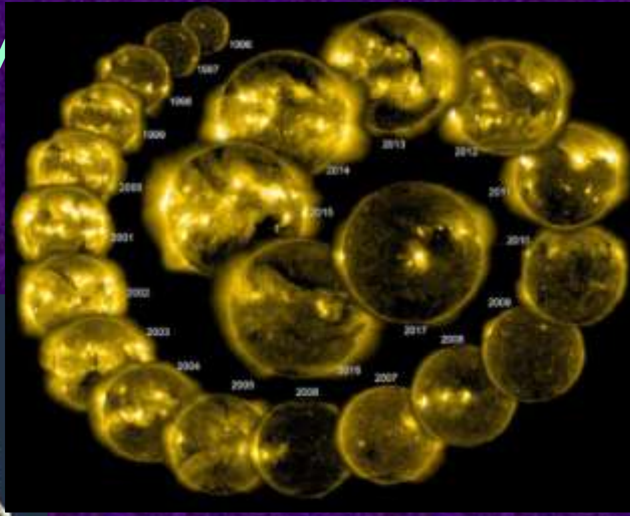

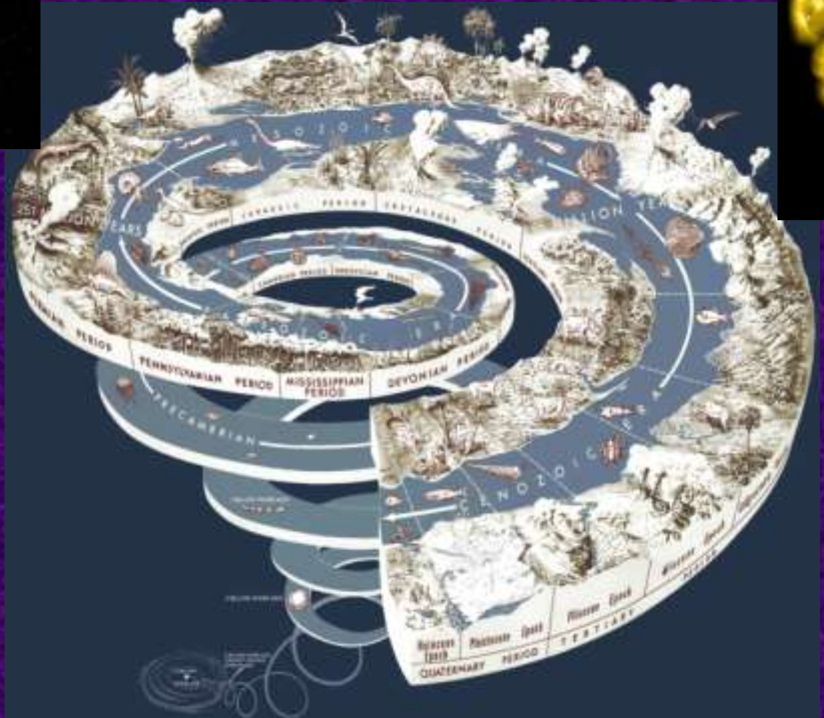

Bulgaria, Sofia,

June 2019

Early Evolution of the Sun: Solar Interior Structure: Luminosity

- *The physics of the solar interior : The energy balance of the standard solar model (SSM) results from equilibrium between nuclear energy production, energy transfer, and photosphere emission*
- *(V. Baturin, A. Oreshina, S. Ayukov, A. Gorshkov, 2017)*
-

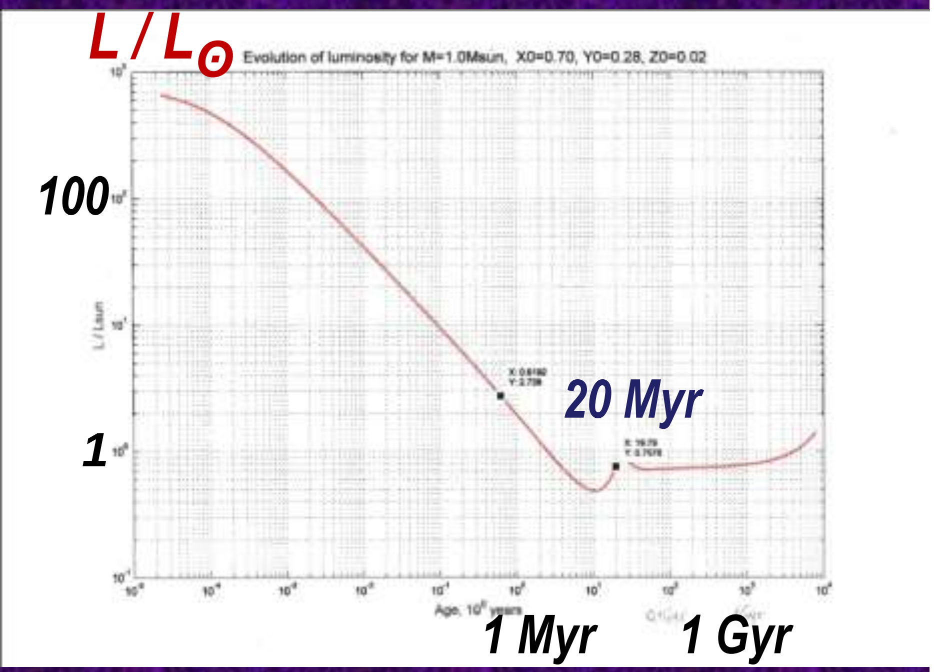

Solar Interior Structure: Radius and T at the bottom of the Convection Zone in the First 20 Myr and until now

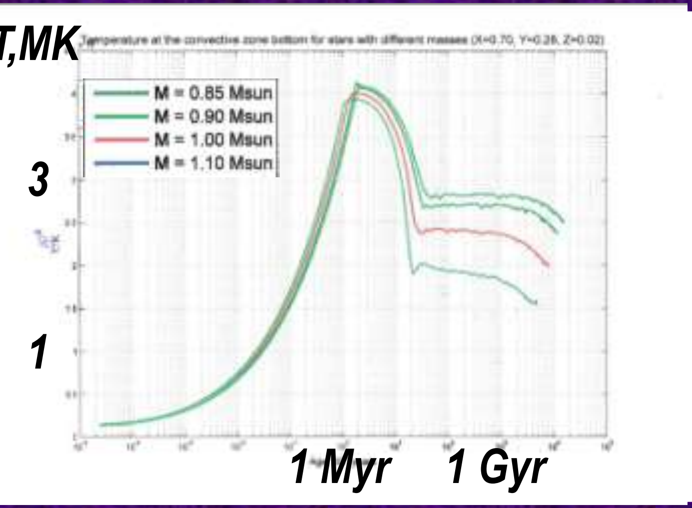

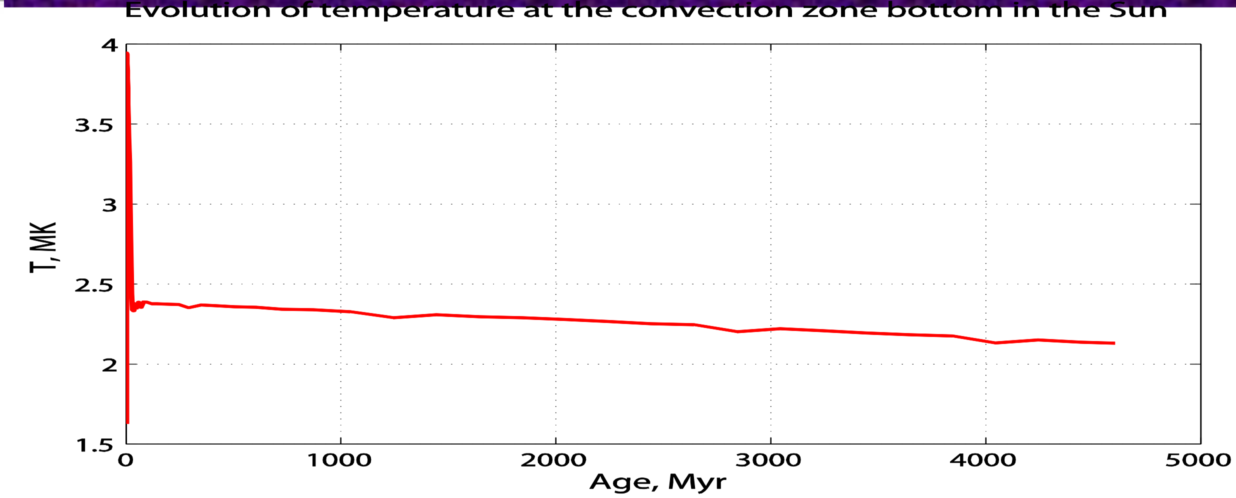

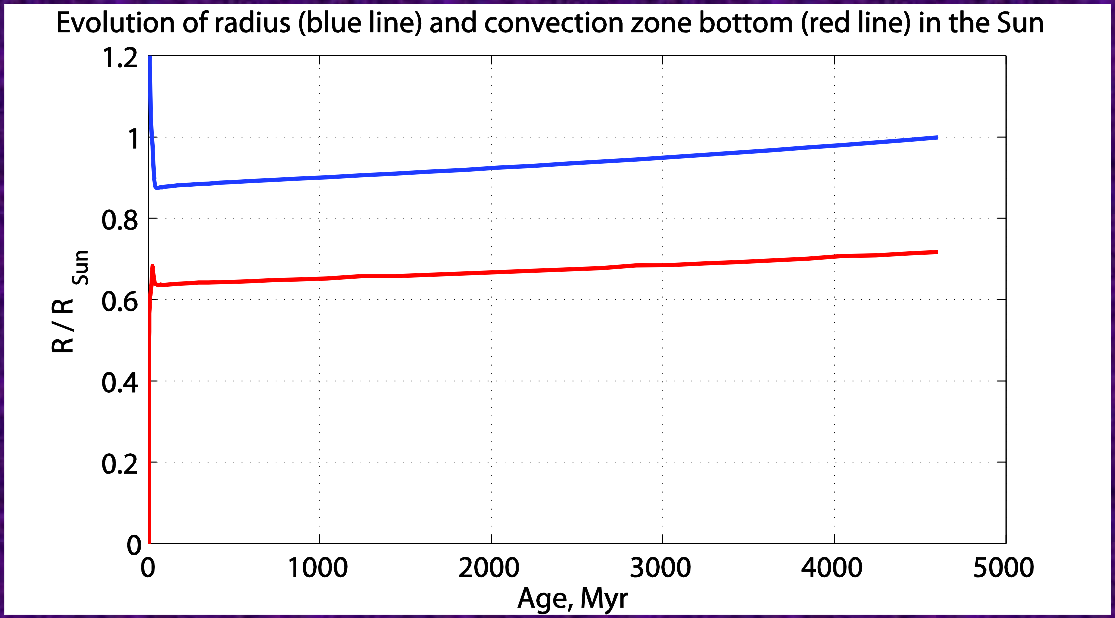

Rotation of a Solar Mass Star at the Stage of Gravitational Contraction

Messina et al. 2011

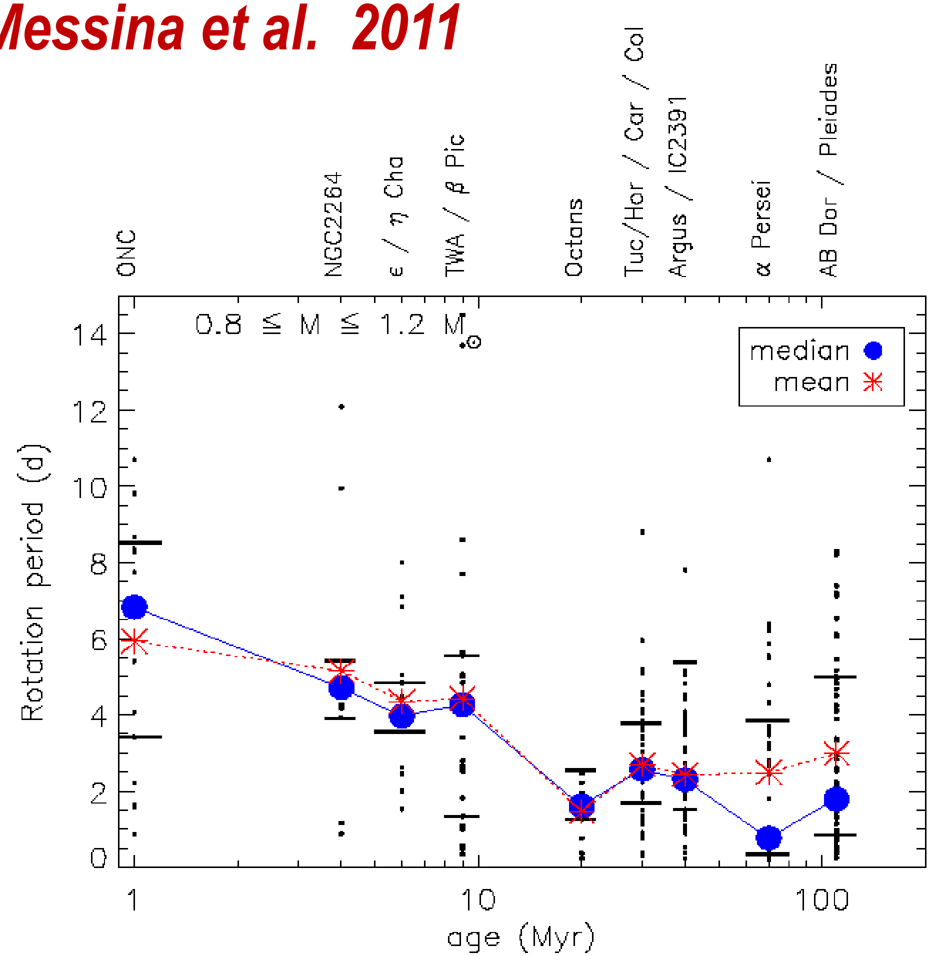

Fig. 7 Rotation period evolution versus time in the 0.8-1.2 solar mass range. Small dots represent individual rotation period measurements. Bullets connected by solid lines are median periods, whereas asterisks connected by dotted lines are mean periods. Short horizontal lines represent the 25th

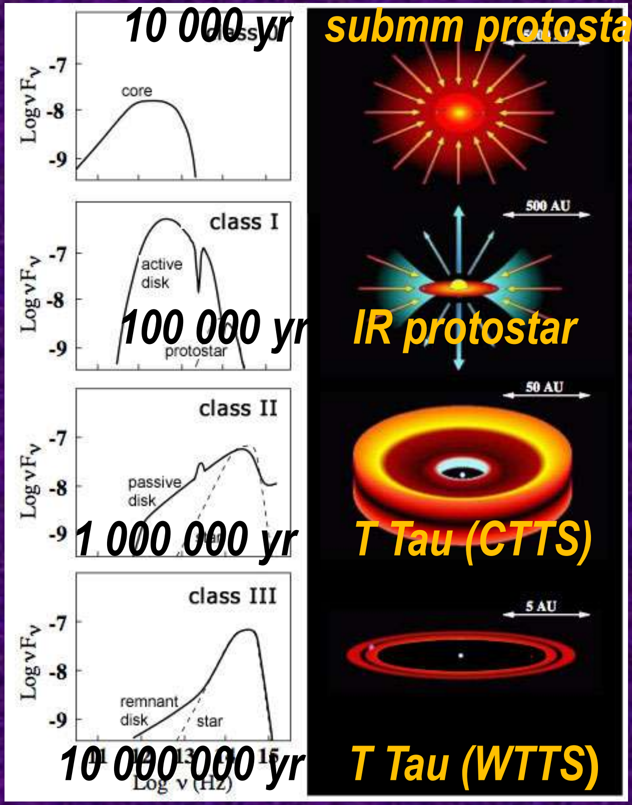

Rotation Period Evolution vs Time in the 0.8-1.2 $M_{\odot}$ range

Rotation as a Main Factor of Stellar Activity

The energy of axial rotation is sufficient to ensure the development of active processes.

$$\frac{GM}{R^2} = \frac{V_{rot}^2}{R}$$

$$\frac{GM}{R^3} = \omega^2$$

$$I = (kR)^2 M$$

$$I\omega = (kR)^2 M\omega = const$$

$$R = \left(\frac{GM}{\omega^2}\right)^{1/3}$$

$$I\omega = k^2 G^{2/3} M^{5/3} \omega^{-1/3} = const$$

$$W_{rot} = \frac{1}{2} I\omega^2 = \frac{1}{2}(0.25 R_\odot)^2 M_\odot (2.9 \cdot 10^{-6})^2 \sim 2.5 \cdot 10^{42}$$

For the Sun, this is $W_{rot} = \frac{1}{2} I\omega^2 =$

$= 1/2 \times (0.25\, R_\Theta)^2\, M_\Theta\, (2.9 \times 10^{-6})^2 \sim 2.5 \times 10^{42}$ erg

This amount of the energy W_{rot} is enough for maintenance the level of the soft X-ray radiation of the active Sun as much as 10^{27} erg/s for $2.5 \times 10^{42} / 10^{27} \times 3 \times 10^7 \sim 10^8$ years

This suggests that the rotation is one of the sources, providing energy costs to maintain the activity.

The missing part of the energy that supports these processes during the next $\sim 10^9$ years, draws from the energy of convective motions, i.e. eventually, from a thermonuclear source in the center of the Sun (or other late-type stars of a similar mass).

The Ages of Members of the Open Clusters and HK Project Stars

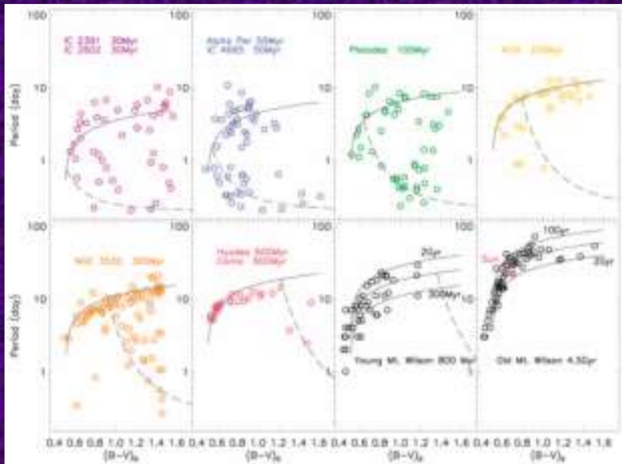

Open clusters contain both fast and slower rotators

Gyrochronology: the Age from P_{rot}

A portion of fast rotating stars decreases versus the age of a cluster

Observational relationships:

Rotation–Age + Activity–Rotation ⇒

⇒ Activity–Age for a star of a given mass

Rotation period of main part of stars in the cluster increases with age

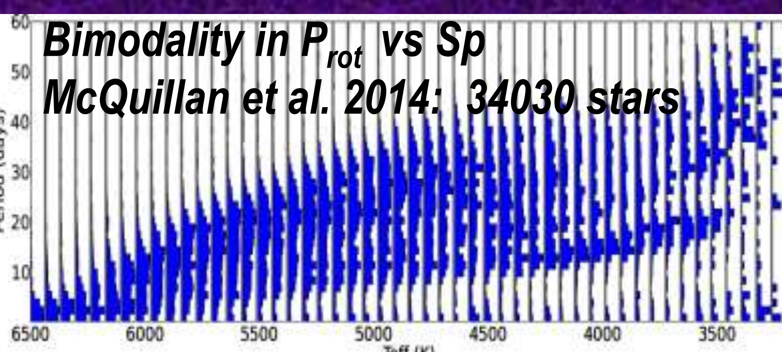

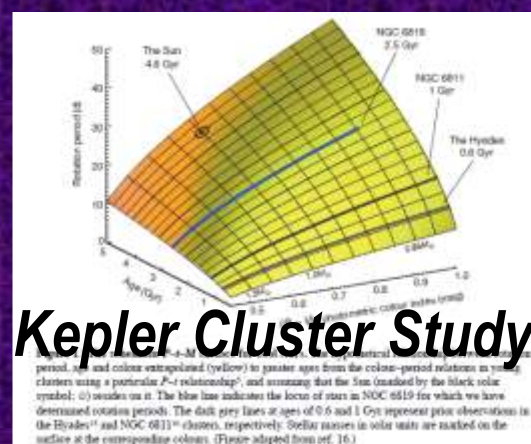

D. Soderblom since 1981 ; S.A. Barnes 2003 ; S. Meibom et al. 2015

G, K and M Stars in Time:

The Sun in Time — The Living with a Red Dwarf

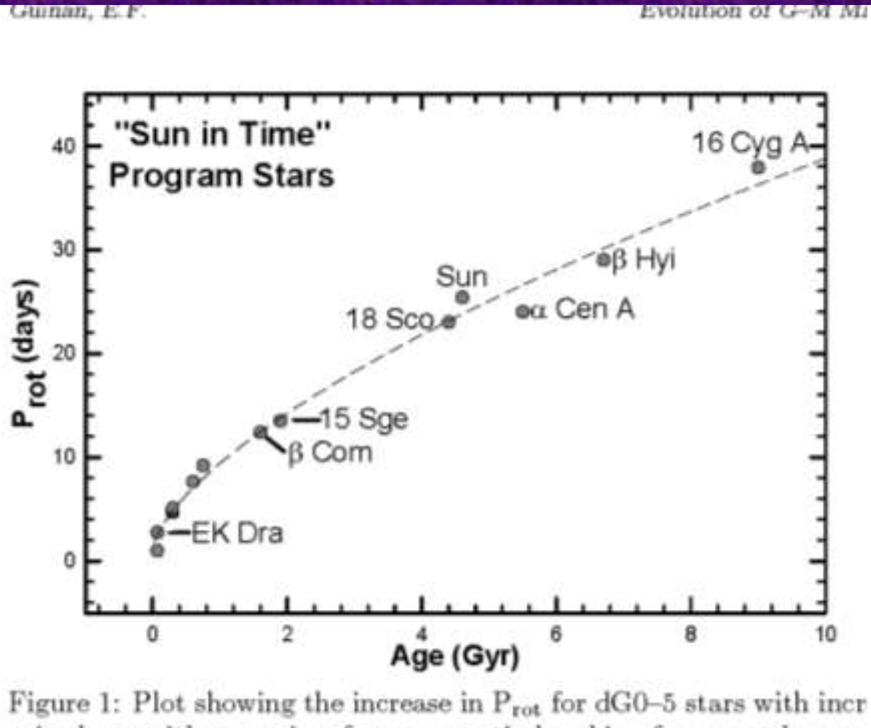

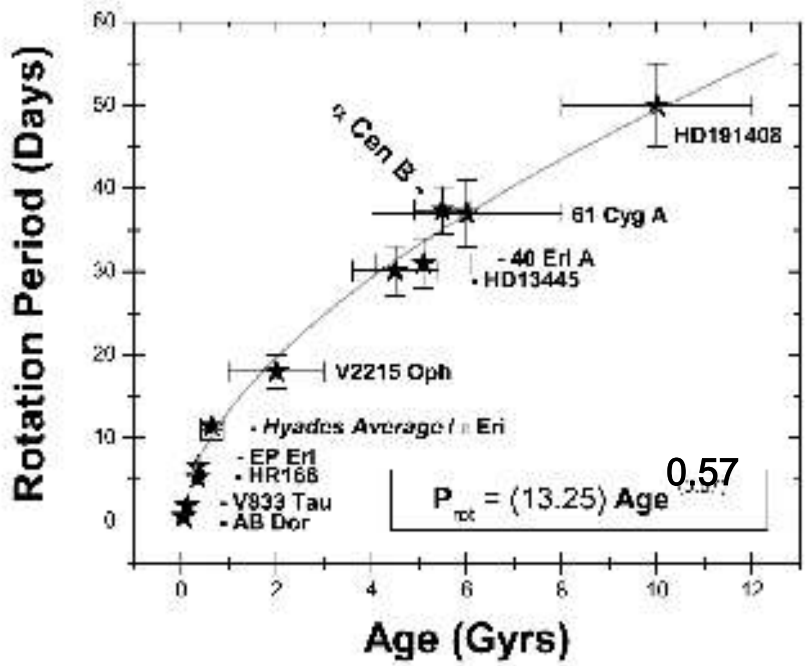

M. Guedel, E. Guinan, S. Skinner 1997; M. Guedel 2004

L.E. DeWarf, K.M. Datin, E.F. Guinan ApJ, 2010

"Rotation - Age" relationship changes weakly for various spectral types (or masses)

The Sun in Time: X-Ray : Stellar Coronae – EM, T

M. Güdel, IAU Symp. 264. 2009

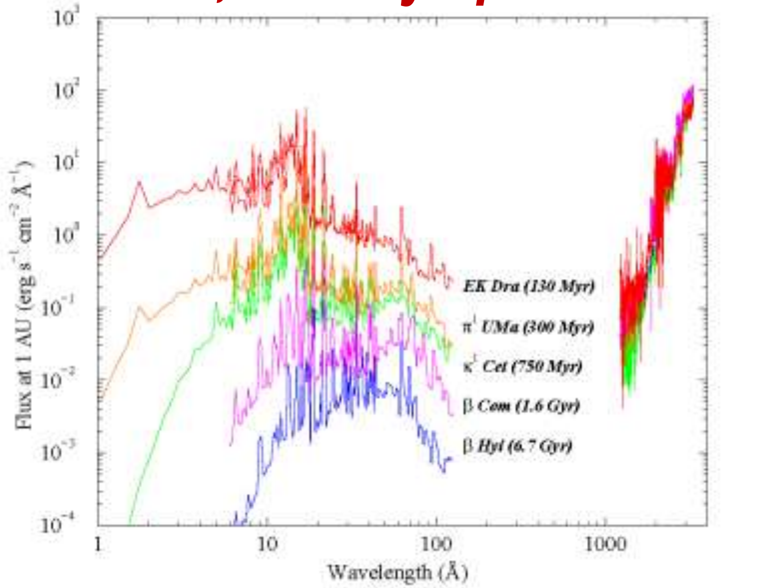

"The Sun in Time"
(G stars from 0.1…7 Gyr)

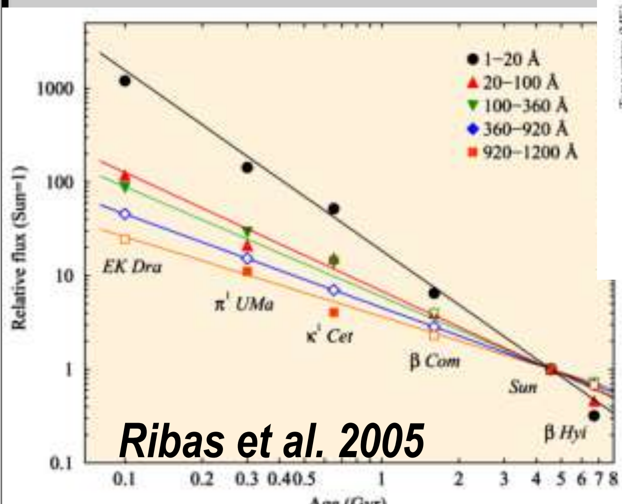

Ribas et al. 2005

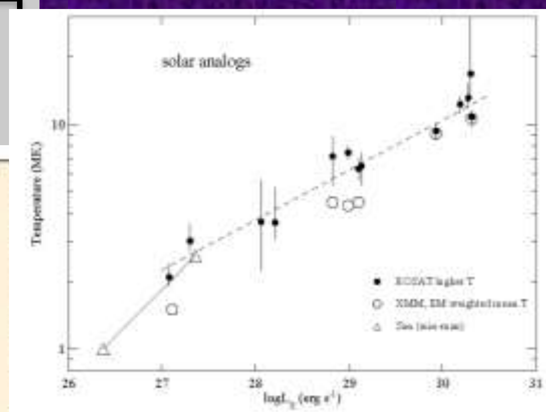

log EM, cm^{-3}

52

50

48

46

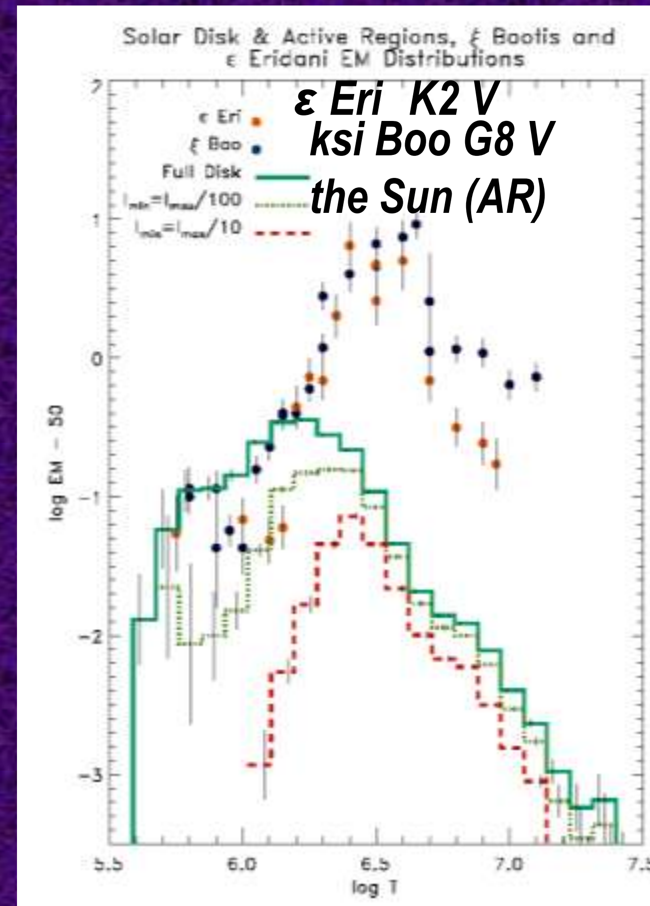

ε Eri K2 V
ksi Boo G8 V
the Sun (AR)

6.0 7.0 log T

M. Güdel. "X-ray astronomy of stellar coronae" Astron. Astrophys. Rev. 2004

FUSE(Far UV Sp Explorer) and GALEX(Galaxy Evolution Explorer)

UV fluxes for 1360 stars NUV 1750 - 2750 A, FUV 1350 - 1750 A

F. Murgas et al. A & A, 2013

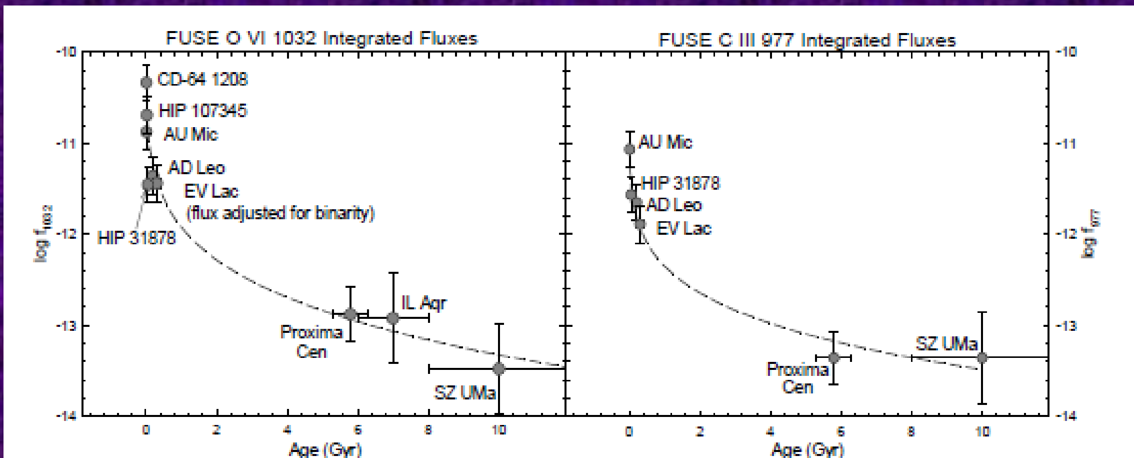

Engle S. G., Guinan E. F. , MizusawaT. 2009

κ^1 Cet (G5 V) P_{rot} = 9 d : a proxy of the Young Sun when life arose on Earth

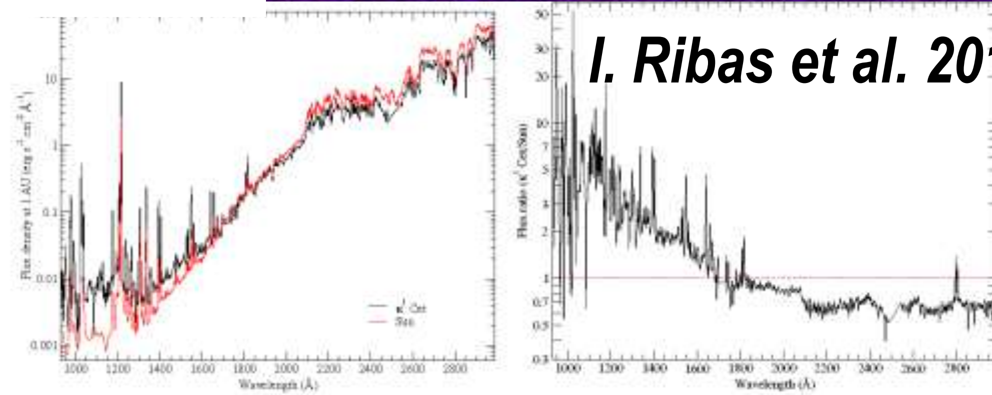

I. Ribas et al. 2010

Figure 7. Left: comparison of the observed UV spectra of κ^1 Cet and the current Sun. Right: ratio of the observed UV spectra of κ^1 Cet and the current Sun. (A color version of this figure is available in the online journal.)

*****

We estimated the FUV-contrast in 1350-1750 A in comparison with the contemporary Sun: It is 2 times for k^1Cet and for the younger G stars – 6 times (Katsova et al. 2017)

Stellar Coronae:
Saturated Regime and Solar-Type Activity

Rotation – Activity $Rx = \log (L_x / L_{bol})$ vs Ro, Rossby number

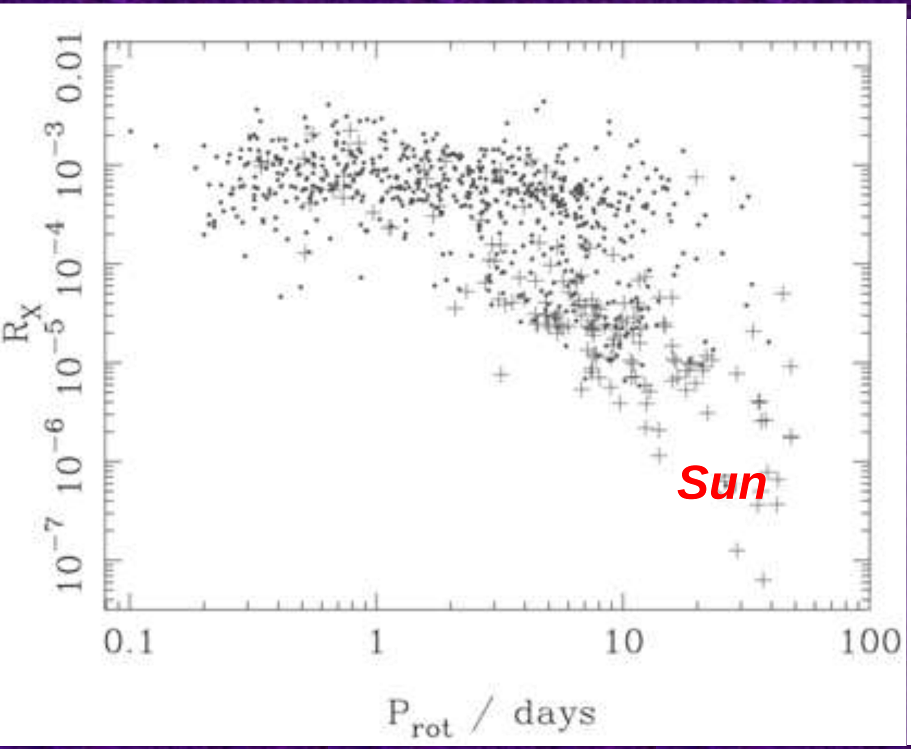

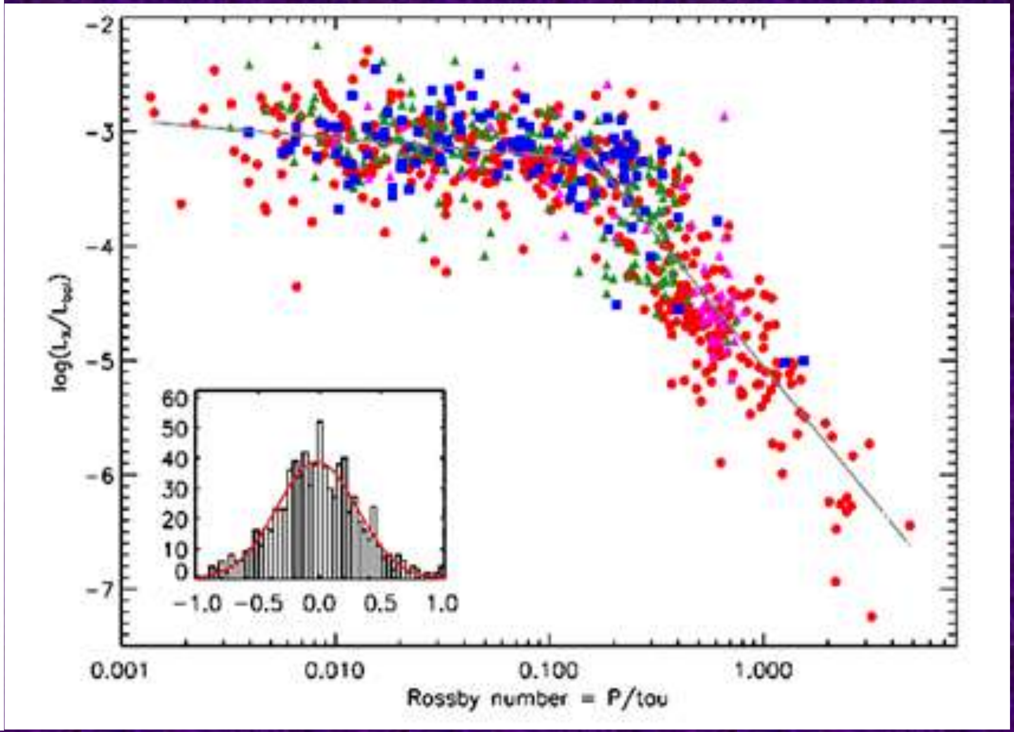

N. Wright et al. 2011 : 824 stars

$Ro = P_{rot} / tau$

A. Reiners et al. 2014

Blue squares: very young stars (up to 50 Myr);
green triangles: young stars (between 85 and 150 Myr);
magenta triangles: intermediate age stars (600–700 Myr);
red circles: field stars

Stellar Coronae

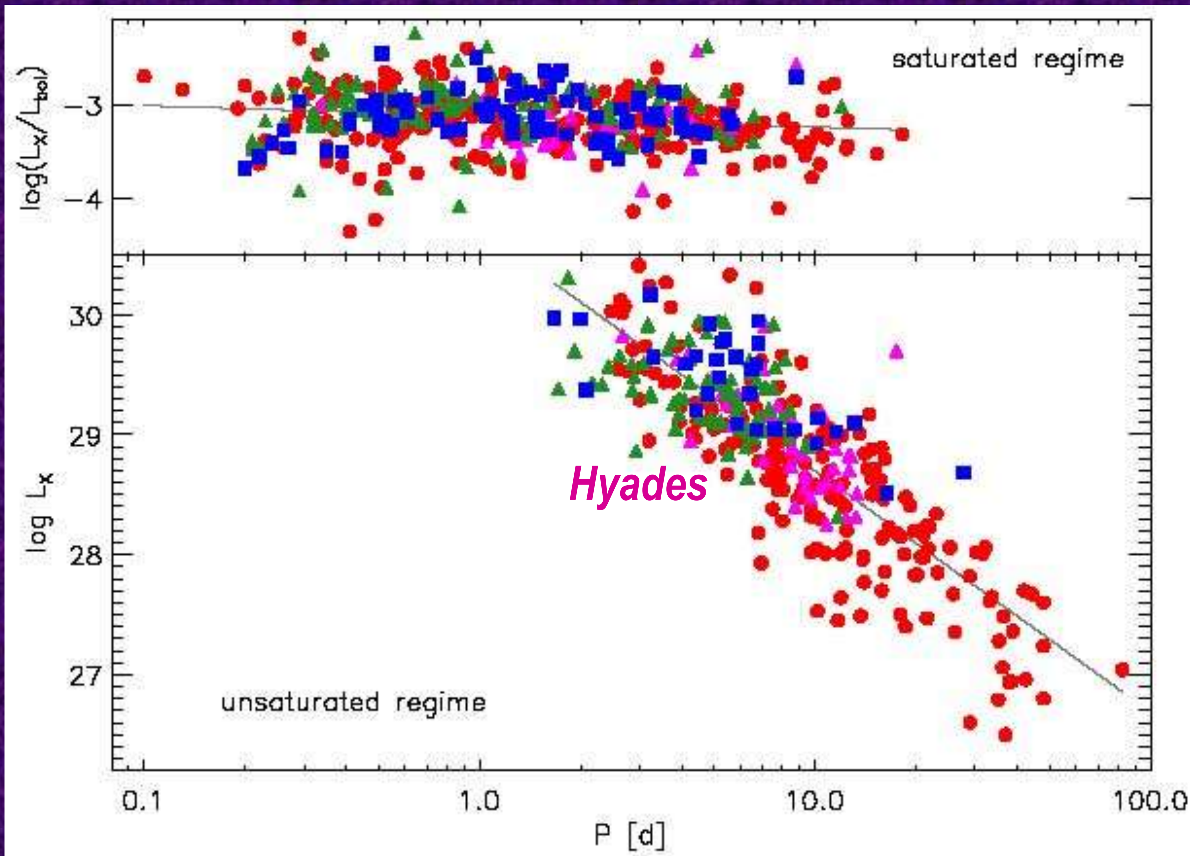

Saturated regime

$$P_{\rm sat}\,[\mathrm{d}] = 1.6\left(\frac{L_{\rm bol}}{L_\odot}\right)^{-1/2} =$$

Unsaturated regime :
solar-type activity ----
determined by the rotation

$L_X \sim v^2$

(Pallavicini et al. 1981)

and it implies formation of a cycle!

Reiners et al. 2014

$$\log L_{\rm X} = (30.71 \pm 0.05) - (2.01 \pm 0.05)\log P,$$

Blue squares: very young stars -- up to 50 Myr;
green triangles: young stars -- between 85 and 150 Myr;
magenta triangles: intermediate age stars 600–700 Myr;
red circles: field stars

The Change in Activity Regime of Stellar Coronae

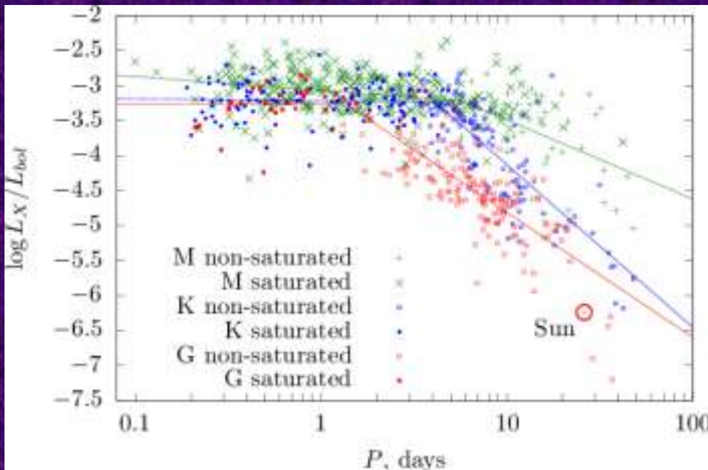

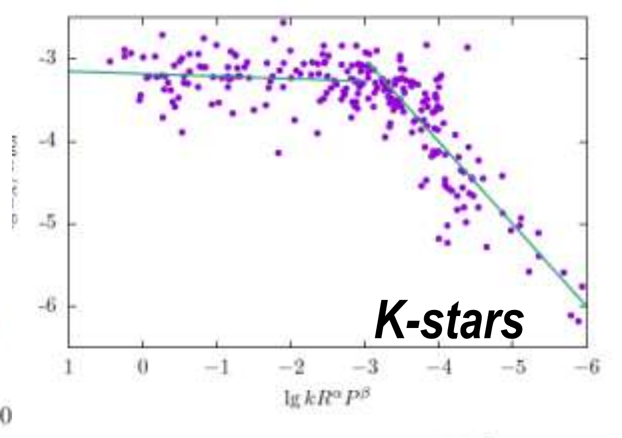

. 1: The coronal activity index vs. $\lg kR^{\alpha}P^{\beta}$ for K stars

Saturated regime changes to solar-type activity at different crucial periods vs Sp

$$P_{\mathrm{sat\,G}} = 1.14 \left(\frac{L_{\mathrm{bol}}}{L_{\odot}}\right)^{-0.61},$$

$$P_{\mathrm{sat\,K}} = 1.88 \left(\frac{L_{\mathrm{bol}}}{L_{\odot}}\right)^{-0.36},$$

$$P_{\mathrm{sat\,M}} = 1.21 \left(\frac{L_{\mathrm{bol}}}{L_{\odot}}\right)^{-0.47},$$

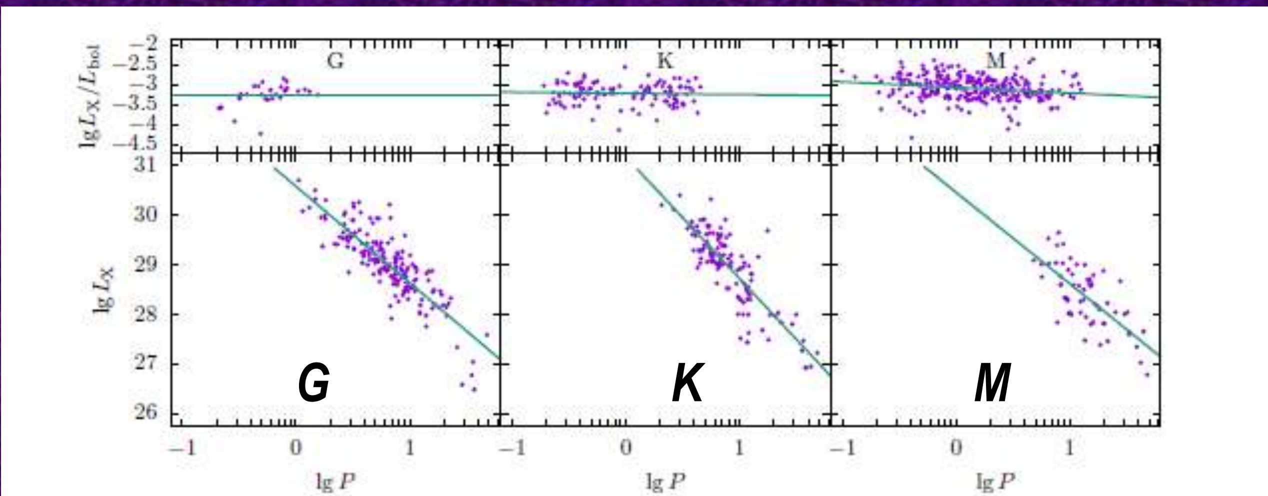

FIG. 2: Coronal activity index vs. logarithm of rotation period for the stars with the saturated activity (upper row) and X-ray luminosity vs. logarithm of rotation period for the stars with the solar-type activity (lower row). See the note on the upper left plot in the text.

Start of cycle formation

G2 V : P_{rot} = 1.1 d

K3 V : P_{rot} = 3.3 d

M4 V : P_{rot} = 7.2 d

Nizamov, Katsova & Livshits, Astron. Letters, 2017

The Chromosphere - Corona Diagram for F, G & K stars

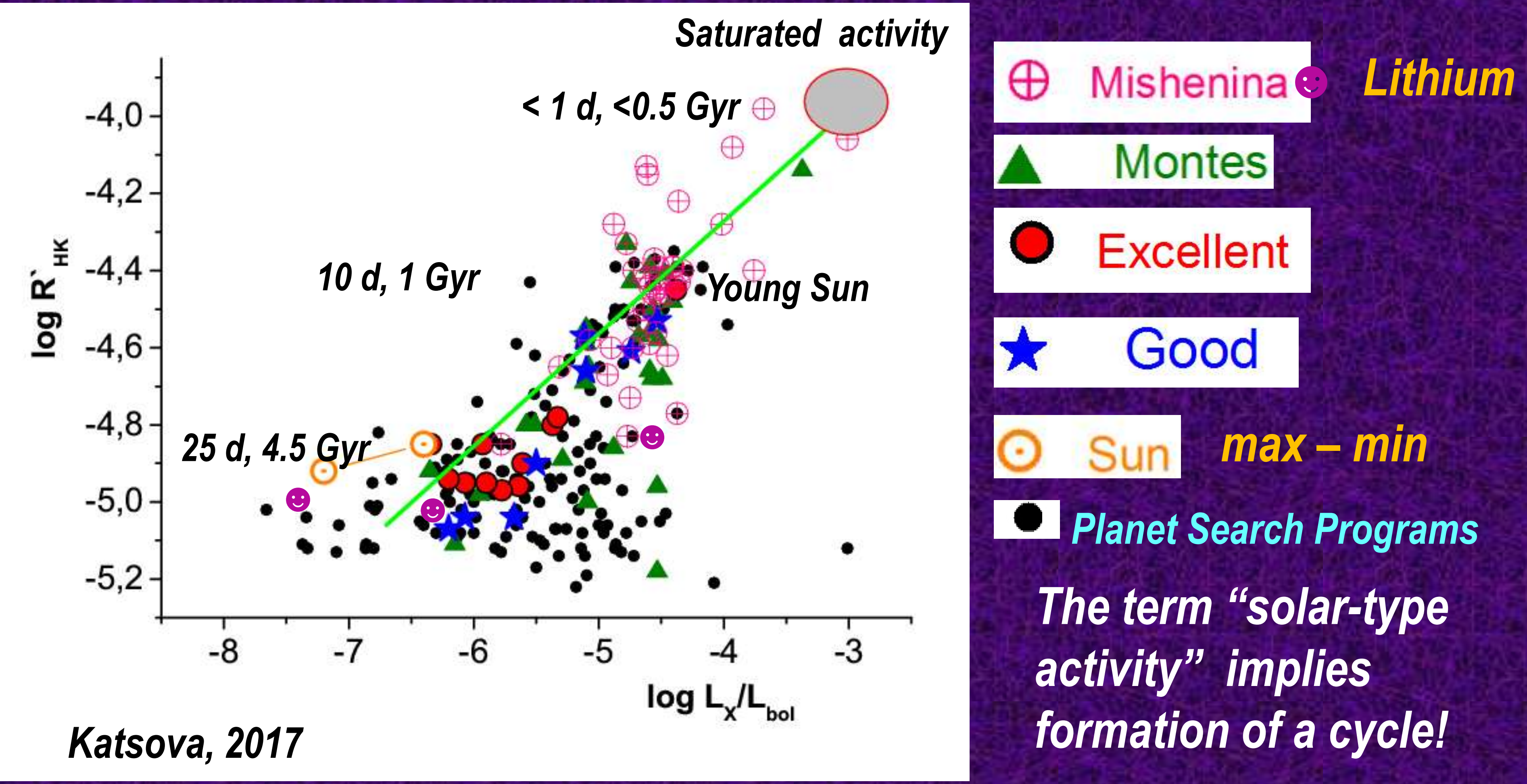

The term "solar-type activity" implies formation of a cycle!

Possible paths of an evolution of solar-type activity

\# E. Mamajek & L. Hillenbrand, 2008 - One-parametric gyrochronology - green lune

\# M. M. Katsova, M.A. Livshits, 2011 Astron Rep ; # M. Katsova, 2011 (JENAM-2011),

\# D. Montes, J. Maldonado, R. Martinez-Arnaiz et al. A & A , 2010, 2011

\# T. Mishenina, C. Soubiran, V. Kovtyukh, M. Katsova, M. Livshits, A & A , **547**, A106, 2012

Cycles and Long-Term Variability of the Sun and Other Stars : HK-Project

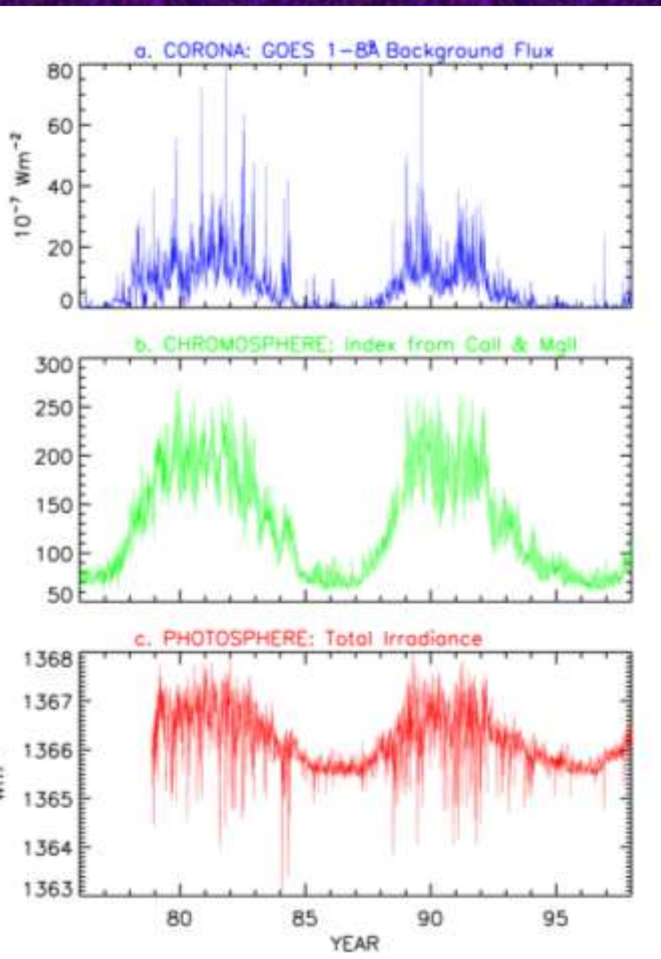

1975 2000

X-rays

Ca II

Total Solar Irradiance

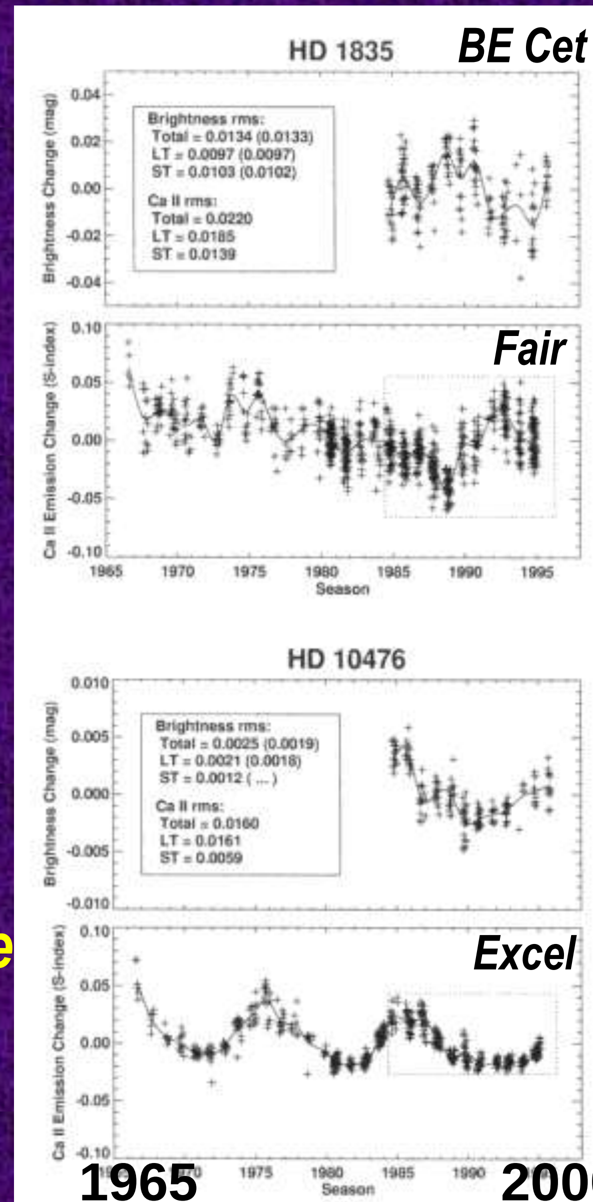

HD 1835 G2 V

P_{rot} = 8 d

P_{cyc} = 9 yr

V –band - phot

anticorrelation

Ca II - chrom

HD 10476 K1 V

P_{rot} = 35 d

P_{cyc} = 9.6 yr

V –band - phot

correlation

Ca II - chrom

Long-Term Evolution of X-rays, H & K Ca II and Magn Activity

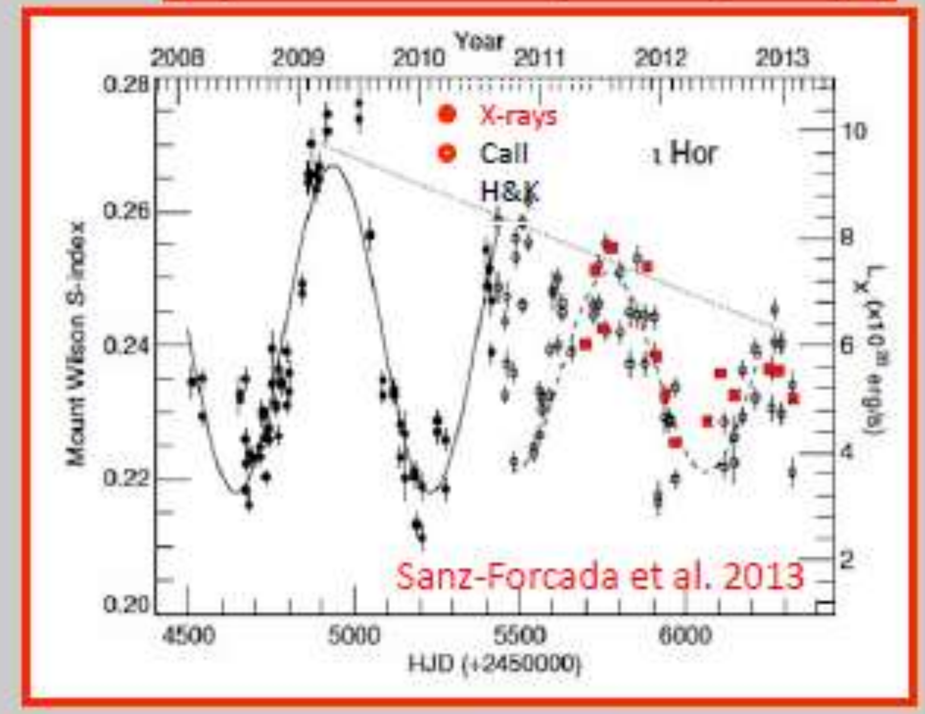

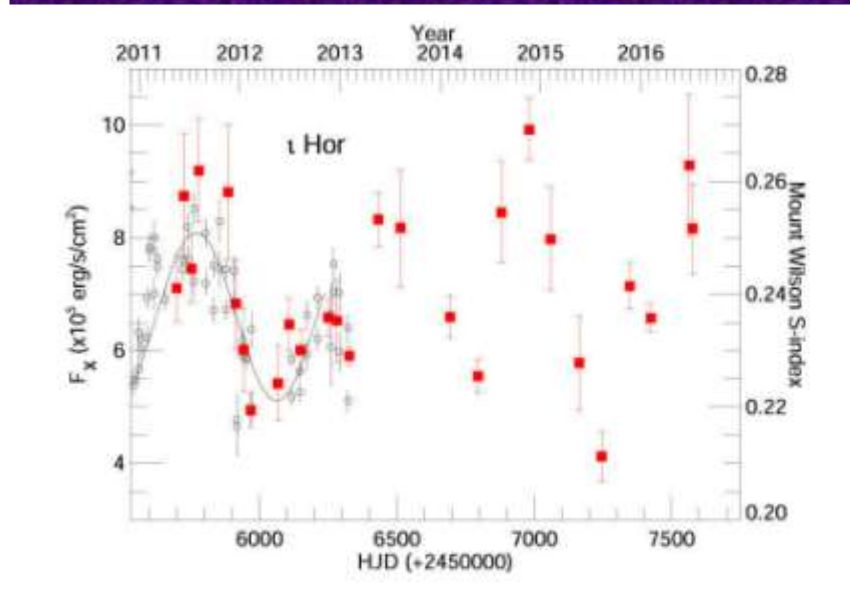

Fig. 2 X-ray and Ca II lightcurve of ι Hor. Black open symbols – Ca II S-index, recent unpublished Ca II data is not shown; red – *XMM-Newton* X-ray flux. Sanz-Forcada et al., in prep.

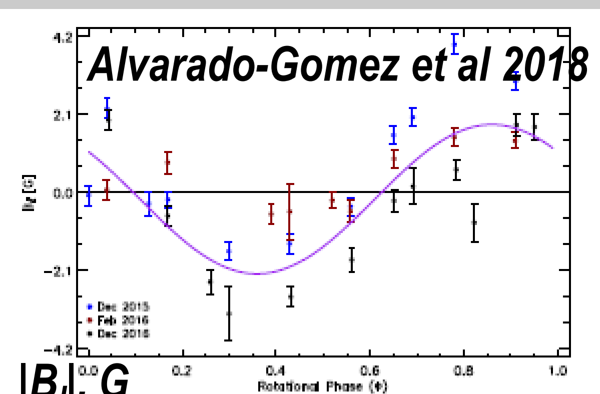

Figure 7. Evolution of the longitudinal magnetic field of ι Hor as a function of rotational phase (with P_{rot} = 7.7 d). Three separate epochs are presented, whose reference $\phi = 0$ dates have been adjusted individually. The solid line (not a fit) shows a phased 7.7-d period sine curve as reference.

Iota Horologium

F8-G0 V (625 Myr)

$B_l = \pm 4$ G

$P_{rot} = 7.7$ d

$P_{cycle} \sim 1.6$ yr

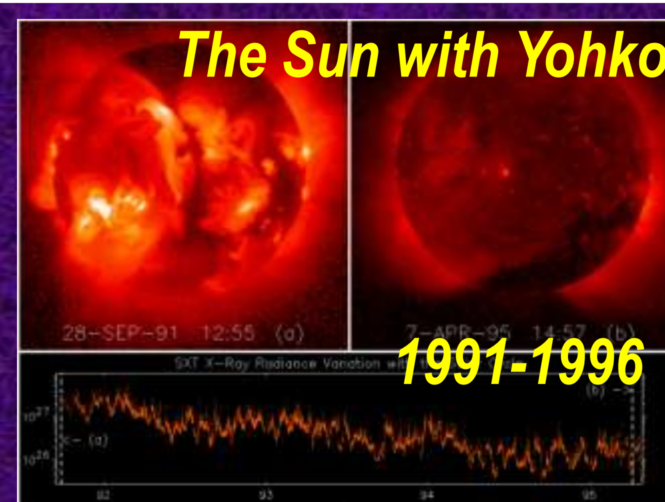

Cycles in Stellar Chromospheres and Coronae

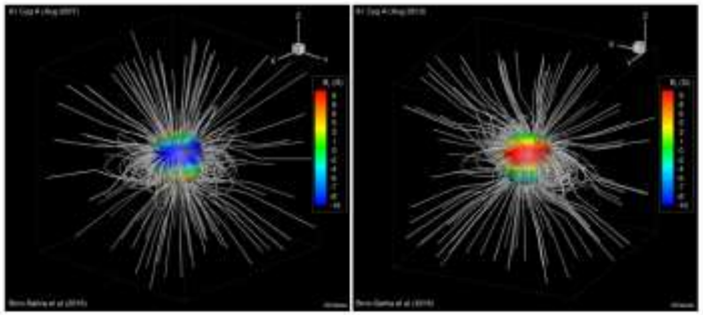

Figure 2: The star 61 Cyg A shows polarity reversals on the large-scale field with a period of a full magnetic cycle (i.e., two reversals) of around 7 years. The reversals are in phase with the chromospheric and coronal cycle. Figure based on the ZDI maps of [29] for Aug 2007 (left) and Aug 2013 (right). The magnetic field lines are extrapolated using a potential field source surface method, which takes into account the radial component of the observed field from [29].

Magnetic 7-yr cycle on 61 Cyg A (A. Vidotto, 2017)

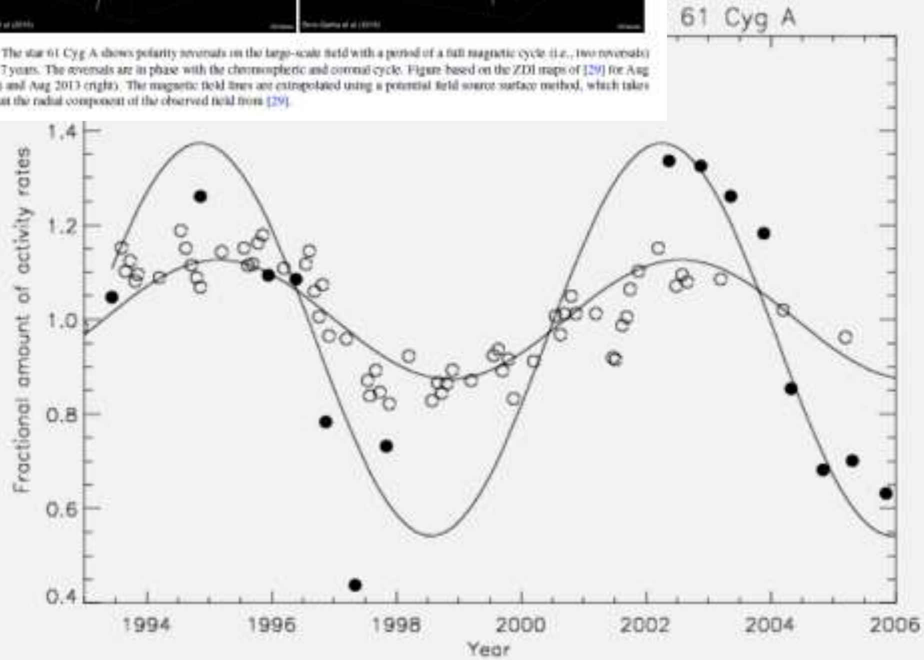

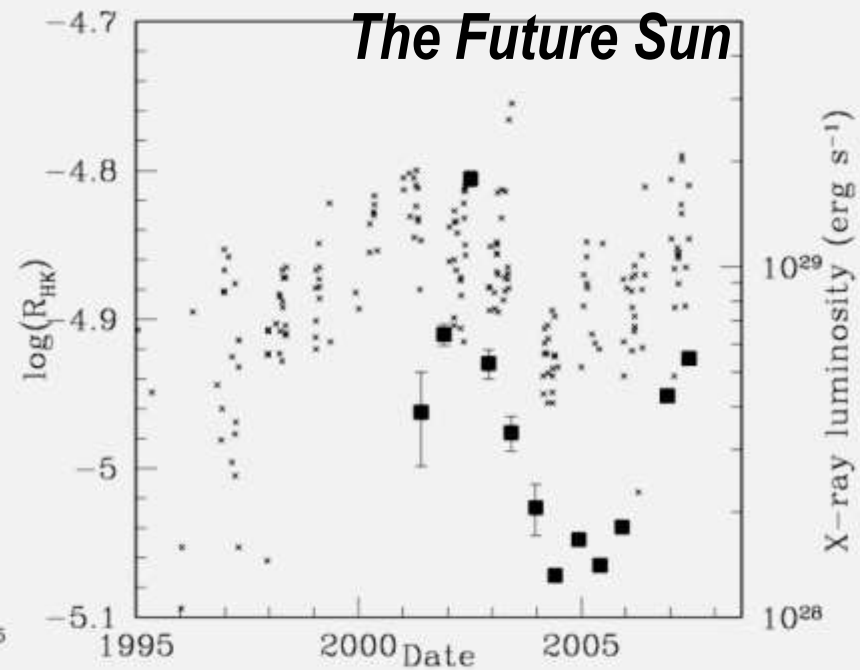

61 Cyg A (K5 V)
P_{rot} = 35 d
P_{cyc} = 7.3 yr Exc

HD 81809 (G2 IV-V)
P_{rot} = 41 d
P_{cyc} = 8.2 yr Exc

I. Pagano, IAU Symp.264, 2009

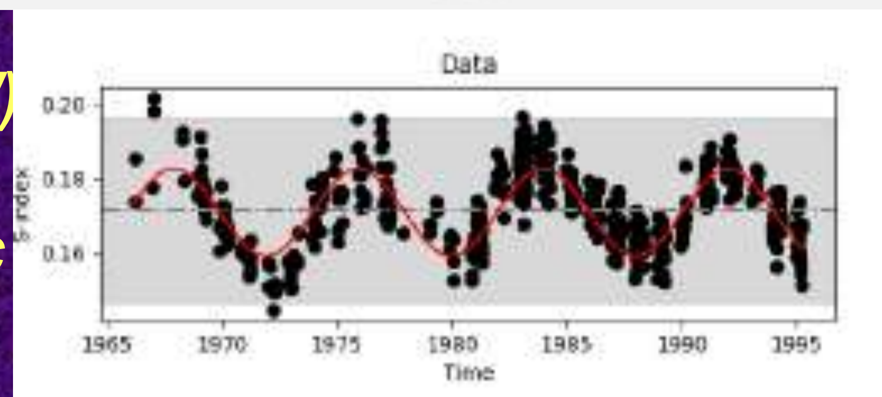

The Magnetic Field of the Young Sun

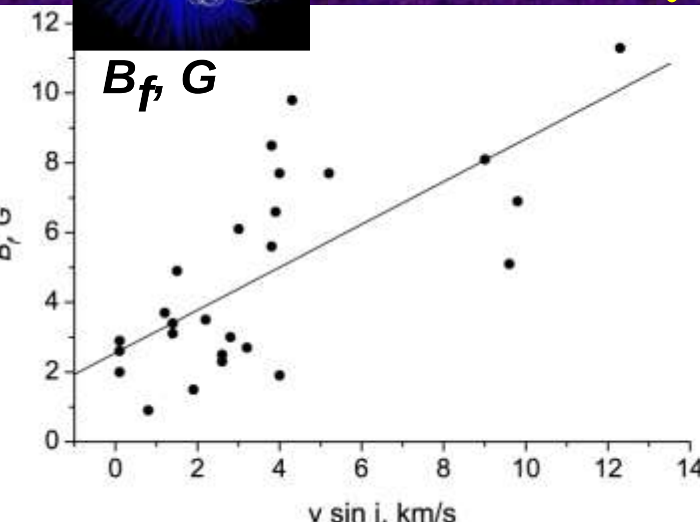

For G-type stars
with P_{rot} = 7 days
$|B_l|$ = 4.72 ± 0.53

L. Rosen et al. 2016

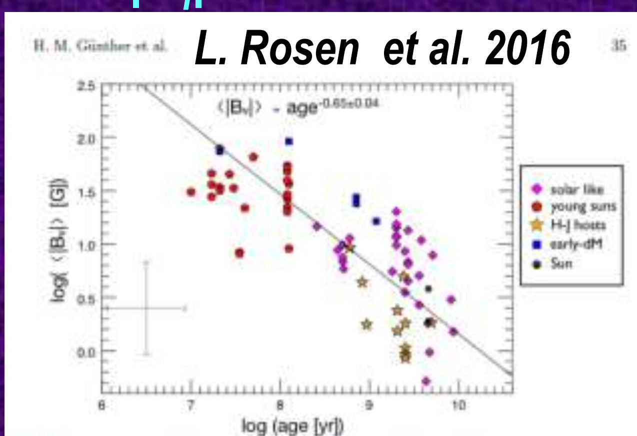

Figure 4: The unsigned average large-scale surface magnetic field ($\langle|B_V|\rangle$) is related to age as $t^{-0.65\pm0.04}$ (solid line) and has a similar power-dependence as the Skumanich law. This magnetism-age relation could be used as a way to estimate stellar ages ("magnetochronology"), although it would not provide better precision than most of the currently adopted age-dating methods.

- Magnetic fields decrease when we pass from fast rotators to slowly rotating stars.
  The total magnetic flux of active solar-type stars exceeds that of the Sun at the maximum of the cycle.
  The total magnetic flux of the current Sun
  10^{24} Mx at the max cycle
  10^{23} Mx at the min cycle
  (Solanki et al. 2002; Vieira & Solanki 2010).
- For the Young Sun
- our estimate is $3 \times 10^{24} \sim 10^{25}$ Mx and
- mean longitudinal magnetic field is - 5 G
- (Bcool collaboration data – Marsden et al. 2014)
- The local magnetic fields in spots of solar-type stars reach 3 – 5 kG
- (Saar 1996; Kochukhov et al., 2010 , Reiners et al 2017 ; Spectropolarimetry)

- The Sun in Time : **Parameters of Activity of Young Suns**

Hot coronae DEM(T):5–8 MK; Density at the base of the corona $3–5×10^9$ cm^{-3}

		P_{rot}	S_{spot},%	L_x,erg/s	R_x	HK-Cycle, yr
Active Sun today	G2 V	25 d	0.3	10^{27}	-7	10-12 Exc

- $|B_l|$ = 0.5 G and $\dot{M} = 3 \times 10^{-14}\ M_\odot$ / year

Siblings of the Young Sun $|B_l|$ = 5 G

BE Cet	G2 V	12	3	10^{29}	-4.4	9 Fair
k^1 Cet	G5 V	9.3 d		10^{29}	-4.4	5.6 Fair
iota Hor	F8 V	7.7 d				1.6
EK Dra	G0 V	2.77 d	10–20	10^{30}	-3	Var

The Alfven radius r = 8.3 $R_\odot$, and $T_w = \dot{M}\ \Omega\ r^2 = 2 \times 10^{32}$ g cm^2 s^{-2}

$\dot{M} = 6 \times 10^{-12}\ M_\odot$ /year (Katsova et al. 2017);

$\dot{M}$ due to CME's on Young Sun is 10% of $\dot{M}$ due to the stellar wind.

This is 20-30 times higher than that for the contemporary Sun.

see also The Solar Wind in Time-3D -Fionnagain, Vidotto et al. 2018, 2019

The Solar Wind in Time_I--II : 3D Stellar Wind Structure

Star	M ($M_\odot$)	R ($R_\odot$)	P_{rot} (d)	Age (Gyr)	$log[L_X]$ (erg/s)	d (pc)
EK Dra	1.04	0.97	2.77	0.12 ± 0.008^a	29.93	34.5
HN Peg	1.10	1.04	4.55	0.26 ± 0.046^b	29.00	17.95
χ^1 Ori	1.03	1.05	4.83	0.5 ± 0.1^c	28.99	186.0
π^1 UMa	1.00	1.00	5	0.5 ± 0.1^c	28.97	14.36
BE Cet	1.09	1.00	12.4	0.6 ± 0.05^d	29.13	20.9
κ^1 Cet	1.03	0.95	9.3	$0.65\pm0.05^{c,d}$	28.79	9.14
β Com	1.10	1.10	12.4	$1.6^{+0.9}_{-0.1}$ ^{e}	28.21	9.13
15 Sge	1.01	1.10	13.5	$1.9^{+1.1}_{-0.9}$ ^{f}	28.06	17.69
18 Sco	0.98	1.02	22.7	$3.0^{+0.2}_{-0.5}$ ^{g}	26.8	13.9
Sun	1.00	1.00	27.2	4.6	≈ 27	1 AU
α Cen A	1.10	1.22	30	$5.5^{+0.0}_{-0.5}$ ^{e}	27.12	1.34
16 Cyg A	1.00	1.16	35	7.0 ± 0.3^h	26.89	21.1

s for each of the simulated s
ses are displayed for base win
ss rates (cf. Figure 2). The ch
lar wind are such to reprodu

Star	n_0 ($10^8 cm^{-3}$)	T_0 (MK)	$\dot{M}$ ($M_\odot yr^{-1}$)
EK Dra	8.8	4.7	1.4×10^{-11}
HN Peg	6.6	3.9	6.9×10^{-12}
χ^1 Ori	6.3	3.8	8.8×10^{-12}
π^1 UMa	6.2	3.7	7.3×10^{-12}
BE Cet	4.8	3.2	3.1×10^{-12}
κ^1 Cet	4.3	3.0	2.0×10^{-12}
β Com	3.6	2.7	1.9×10^{-12}
15 Sge	3.4	2.6	2.1×10^{-12}
18 Sco	2.5	1.9	2.8×10^{-13}
Sun	2.2	1.5	3.5×10^{-14}
α Cen A	2.1	1.4	4.5×10^{-14}
16 Cyg A	1.9	1.1	8.1×10^{-15}

Table 1. Stellar parameters of our sample are shown on the left (mass, radius, rotation period, age, and distance) and specifics of the simulations are shown on the right (base density, base temperature, mass-loss rate, angular momentum-loss rate, open magnetic flux, and flux ratio between surface and open magnetic fluxes). Stellar parameters were compiled in Vidotto et al. (2014b). Distances are found using the Gaia DR2 database[a] (Prusti et al. 2016; Brown et al. 2018) values for parallax.

	Observables						Simulation					
Star	$M_\star$ ($M_\odot$)	$R_\star$ ($R_\odot$)	P_{rot} (d)	Ω ($\Omega_\odot$)	Age (Gyr)	d (pc)	n_0 (cm^{-3}) ($\times10^8$)	T_0 (MK)	$\dot{M}$ ($M_\odot$/yr) ($\times10^{-13}$)	$\dot{J}$ (ergs) ($\times10^{30}$)	Φ_{open} (G cm) ($\times10^{22}$)	f
χ^1 Ori	1.03	1.05	4.86	5.60	0.5	$8.84^{\pm0.02}$	18.9	2.84	46.5	285	22.5	0.37
HD 190771	0.96	0.98	8.8	3.09	2.7	$19.02^{\pm0.01}$	13.2	3.04	36.1	91.0	23.46	0.59
κ^1 Ceti	1.03	0.95	9.3	2.92	0.65	$9.15^{\pm0.03}$	12.8	2.98	22.1	124	30.71	0.44
HD 76151	1.06	0.98	15.2	1.79	3.6	$16.85^{\pm0.01}$	9.54	2.47	8.26	31.8	14.68	0.49
18 Sco	0.98	1.02	22.7	1.20	3.0	$14.13^{\pm0.02}$	7.5	1.85	6.47	5.34	4.29	0.70
HD 9986	1.02	1.04	23	1.18	4.3	$25.46^{\pm0.03}$	7.44	1.82	5.82	2.35	3.30	0.94
Sun Min	1.0	1.0	27.2	1	4.6	-	6.72	1.5	1.08	1.04	3.44	0.69
Sun Max	1.0	1.0	27.2	1	4.6	-	6.72	1.5	1.94	15.5	6.17	0.24

[a] https://gea.esac.esa.int/archive/

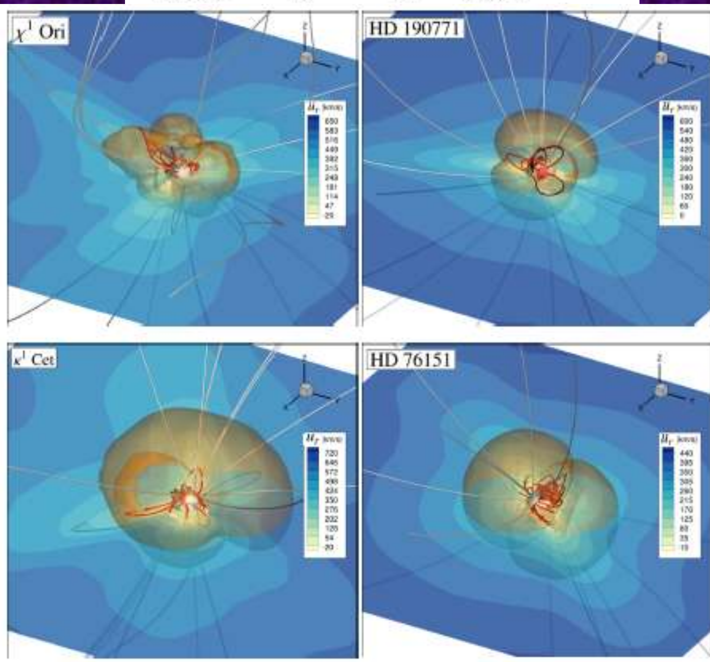

Figure 2. Steady state solutions for the simulated winds of the solar analogues. The translucent slice through the z=0 plane shows the wind radial velocity (u_r). Open and closed magnetic field lines are shown as grey and red streamlines respectively. Magnetic polarity is shown on the stellar surface as a red-blue diverging contour. The orange surface shows the Alfvén surface, where $u_r = u_A$, the Alfvén velocity. Note that the faster rotators have much less uniform, dipolar Alfvén surfaces, due to the less uniform magnetic fields topologically, at their surfaces.

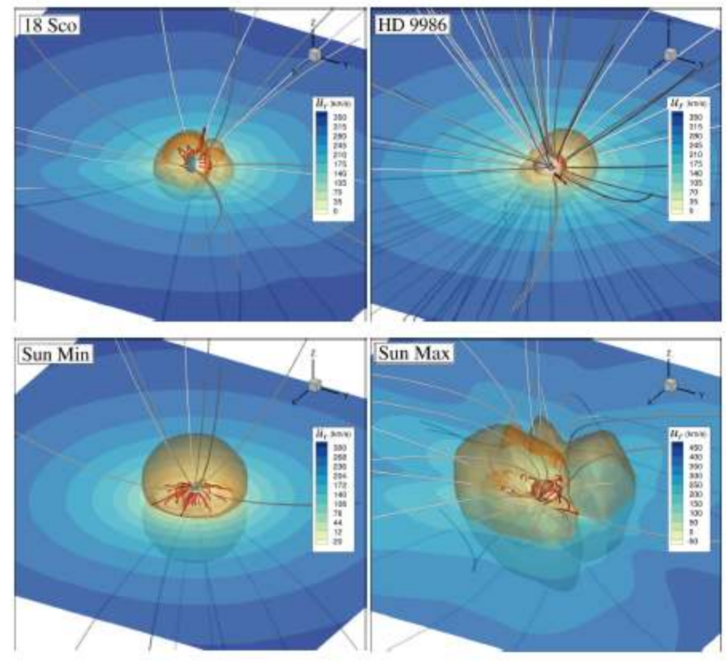

Figure 2. (cont.) Steady state solutions for the simulated winds of the solar analogues, showing the slower rotators in our sample.

Fionnagain, Vidotto et al. MNRAS 2018, 2019

Some Extreme Energetic Flares on the Sun

The 1-2 Sept 1859 --- Carrington Flare (~ X45)

February 1956

August 1972

March 1989

June 1991

Oct-Nov 2003 (4.Nov - X28)

… 6. Sept 2017 - X9.3

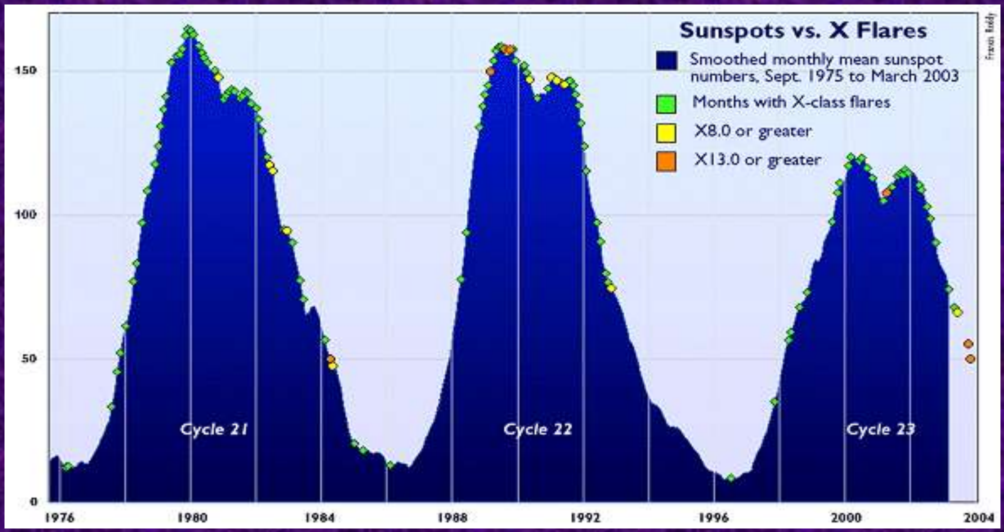

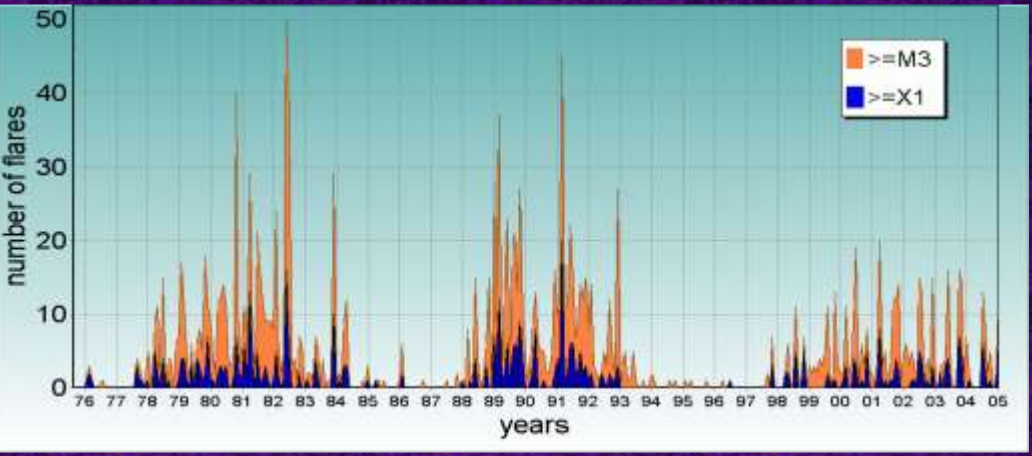

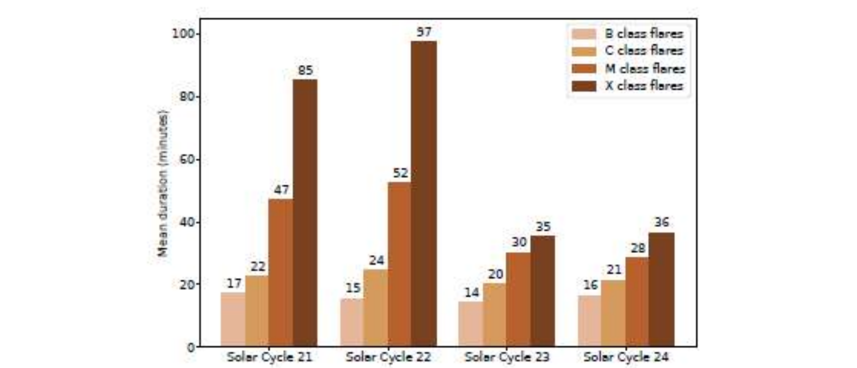

B.Swalwell et al. 2018

Figure 1: Mean reported duration (in minutes) of flares of different classes in each of the last 4 solar cycles as derived from the GOES SXR list. From left to right bars represent B-class flares, then C-class, M-class, and X-class.

Flares stronger than $3 \cdot 10^{32}$ erg can not occur on the contemporary Sun (Katsova & Livshits 2015; Katsova et al. 2018)

Solar Extreme Events in the Past:

The strongest events over the Holocene (the current interglacial period started about 11 000 yrs ago):

 # ~ 640 BC (O'Hare et al. PNAS, 2019)

 # 774 / 775 AD (40× the strongest SEP event of the instrumental era 23. Febr 1956)

 # 993 / 994 AD (0.6 weaker than previous event)

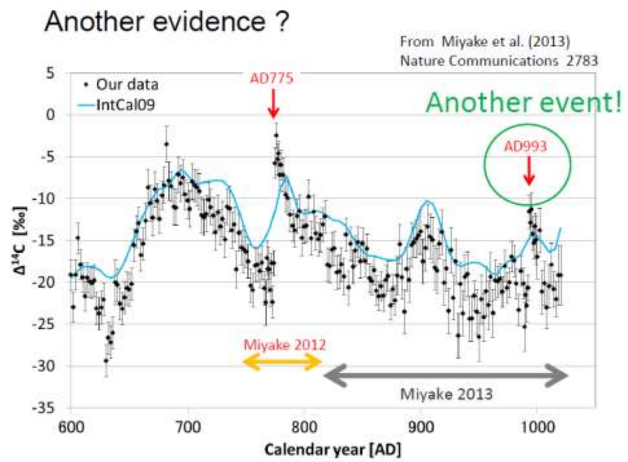

Miyake et al. 2019 (GeophysRL) observed a ~50% increase in ^{10}Be concentration around 994, consistent with the Greenland data. Increases in ^{10}Be concentrations in both hemispheres support a solar origin of the 994-event.

Cosmogenic proxies:

 # C-14 (radiocarbon) - dendrochronology

 # Be-10 and Cl-36 - in polar ice cores

Because the half-life of C-14 is only 5730 yrs, this dating method is used only for dating things that lived within the last 50 000 yrs.

Problem: Low time resolution (annual at best)

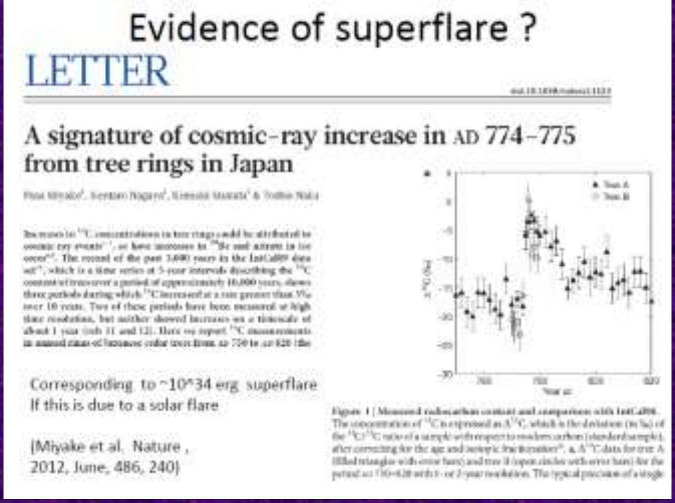

10^{36}-10^{37} erg -- V410 Tau (dK3e)

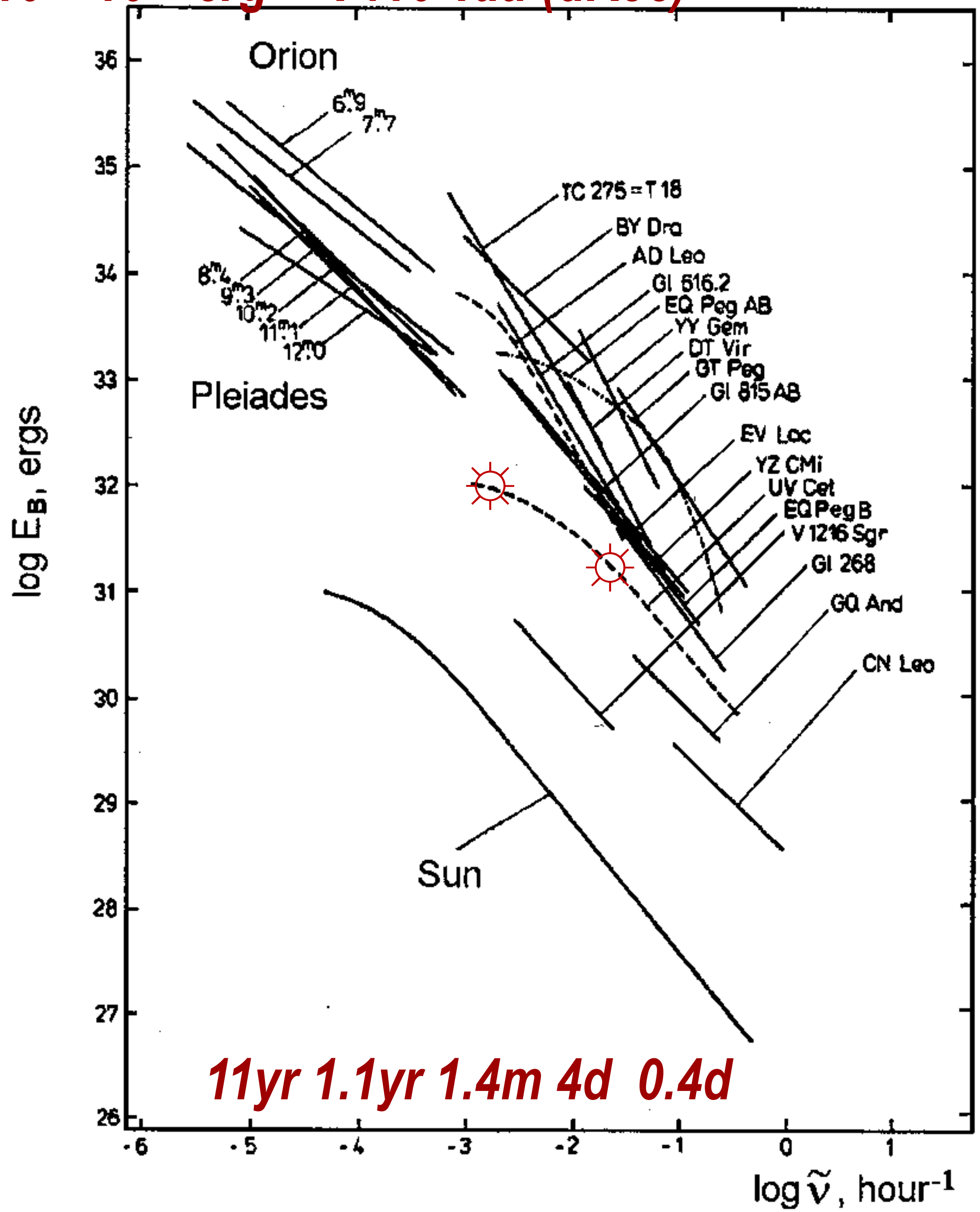

Pre-Keplerian Epoch

Flare Occurrence Frequency on Red Dwarf Stars

(Gershberg 1987, 2005)

☼ The Sun :

X - and M - flares at the maximum 1979–1981

Impulsive flares on late-type dwarf stars have the same *magnetic origin* as those on the Sun

The Kepler Mission

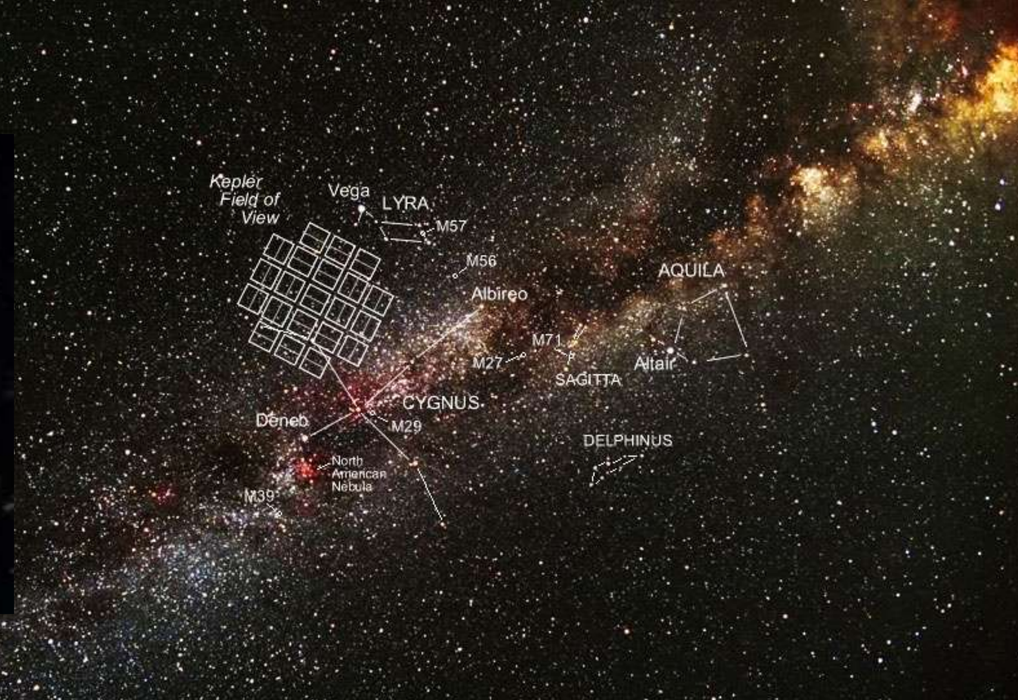

March 7, 2009
Cape Canaveral

Deactivated on November 15, 2018

1.4 m- primary mirror
0.95 m -Schmidt telescope
430–890 nm
42 CCDs in focal plane
100 sq deg

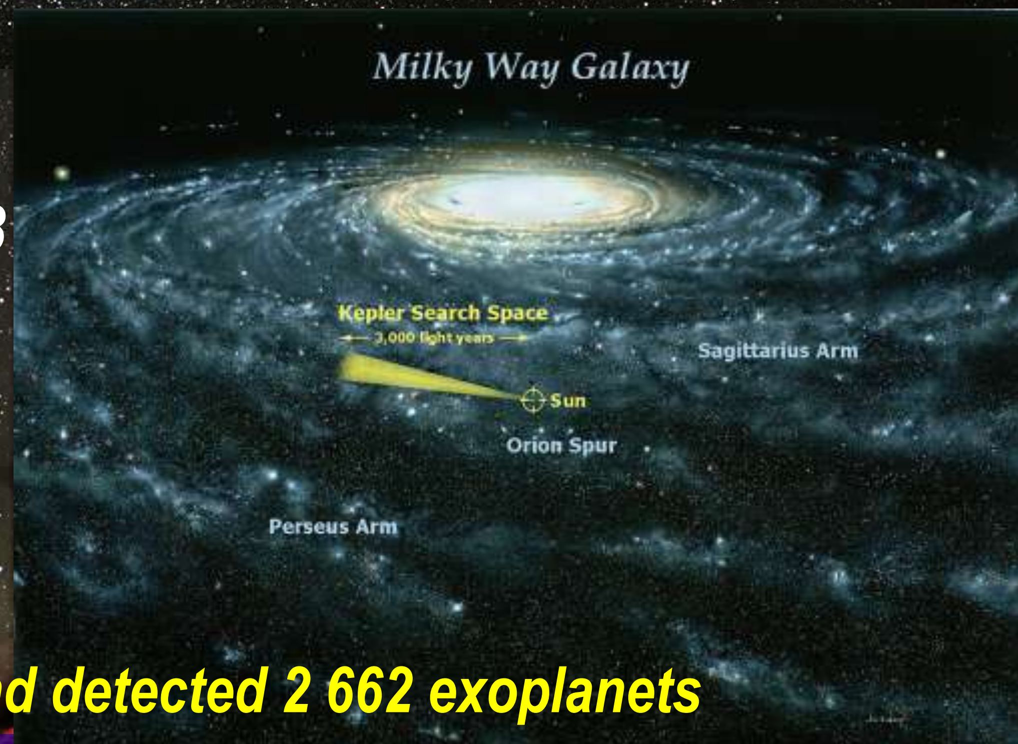

Kepler observed 530 506 stars and detected 2 662 exoplanets

STELLAR FLARES OBSERVED IN LONG-CADENCE (30-min) DATA FROM THE KEPLER MISSION

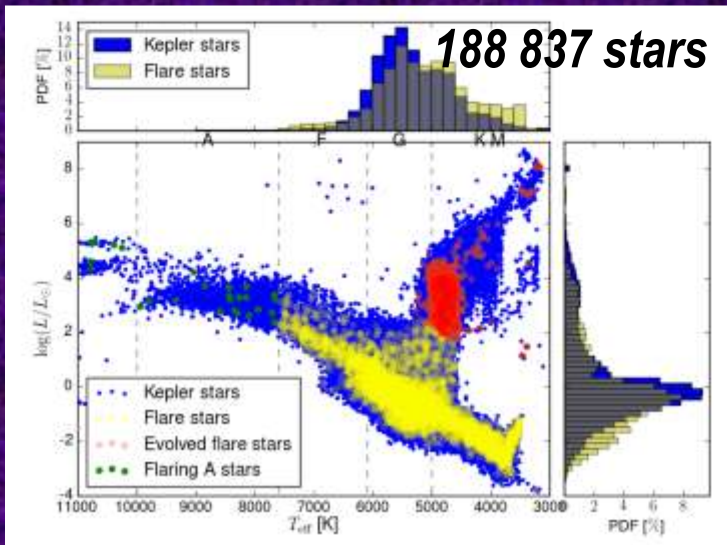

> 40%
of the original
solar-type
superflare stars
in previous
studies are now
classified
as subgiants

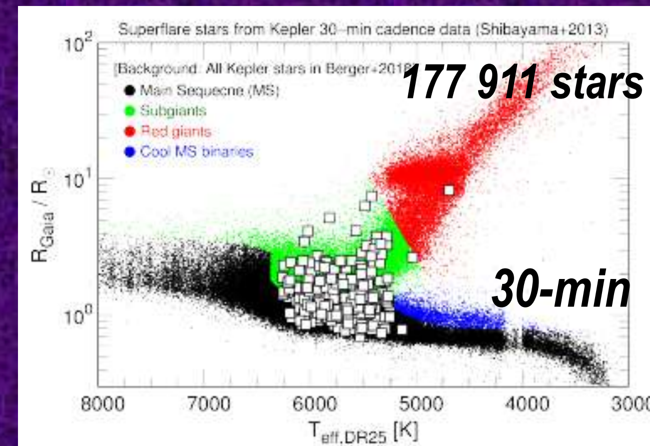

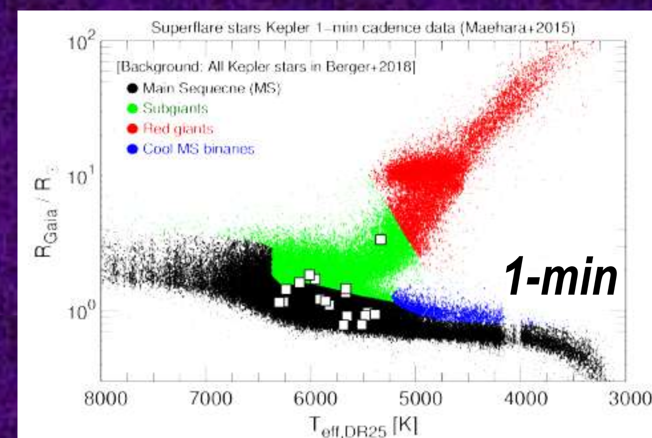

Sp	# Objects	# Flare stars	# Incidence
A+B	2141	28	1.31%
F	22107	708	3.20%
G	116178	3365	2.90%
K+M	48411	2556	5.28%
giants	22837	653	2.86%

Notsu et al. arXiv 2 Apr 2019

Van Doorsselaere et al. arXiv 7 Nov 2017, Yang & Liu, arXiv 4 March 2019

Samples of the Kepler Light Curves

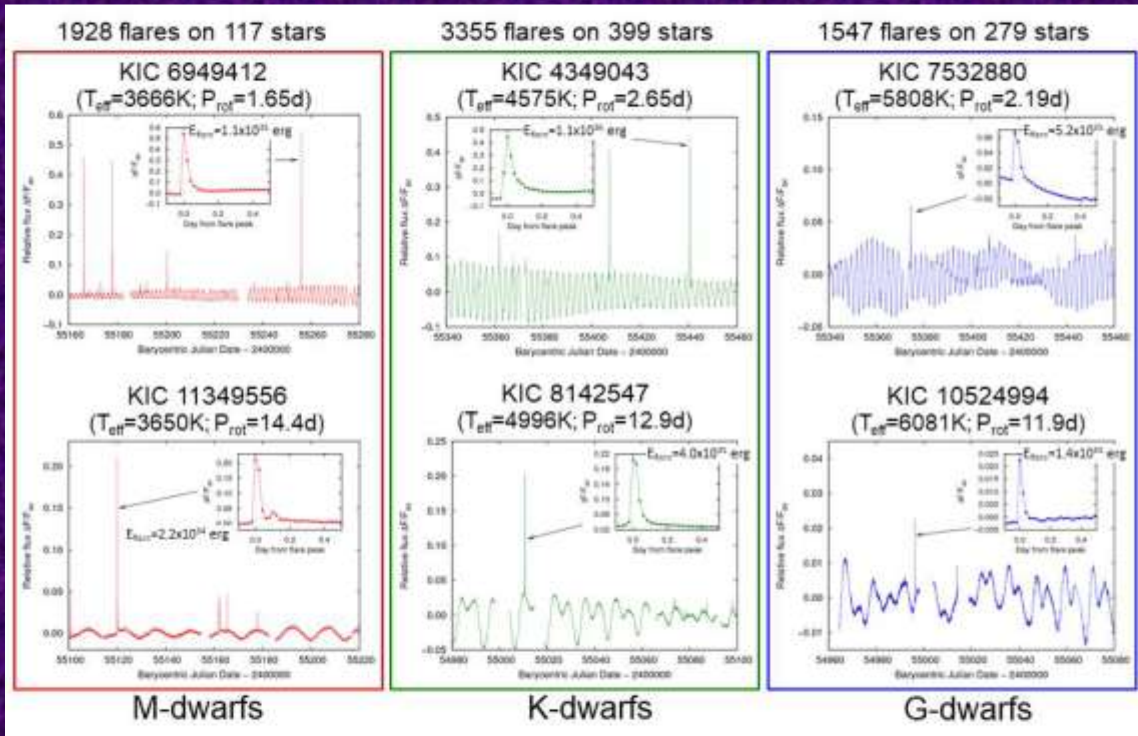

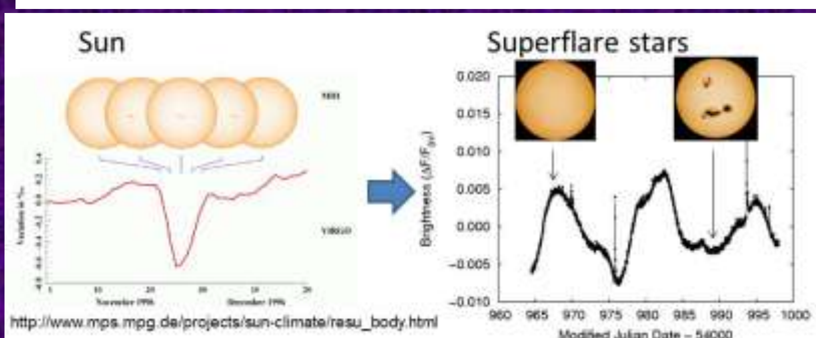

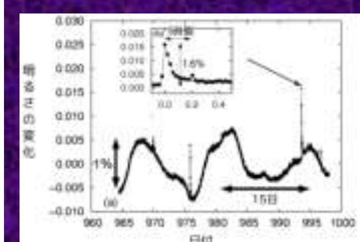

$$S^{*}_{\rm spot} = \left(\frac{R_{\rm star}}{R_{\odot}}\right)^{2} \frac{T^{4}_{\rm star}}{T^{4}_{\rm star} - \{T_{\rm star} - \Delta T(T_{\rm star})\}^{4}} \frac{\Delta F}{F},$$

- *The typical duration of detected flares is ~ 0.1 d*
- *⇒ The amplitude A of the largest flares depends on T_{eff}*
- ◇ M dwarfs: 100%
- ◇ K dwarfs: ~50%
- ◇ G dwarfs: < 10 %
- *⇒ The bolometric energy released by flares ranges from 10^{32} to 10^{36} erg.*

Rotation Periods: 0.5—30 days

⇒ Amplitudes Δ F/F : 0.1—20%

Maehara et al. Cool Stars20, 2018

General Pattern : The Flare Energy E_{flare} and Starspot Area, A

Flare activity depends on spot size

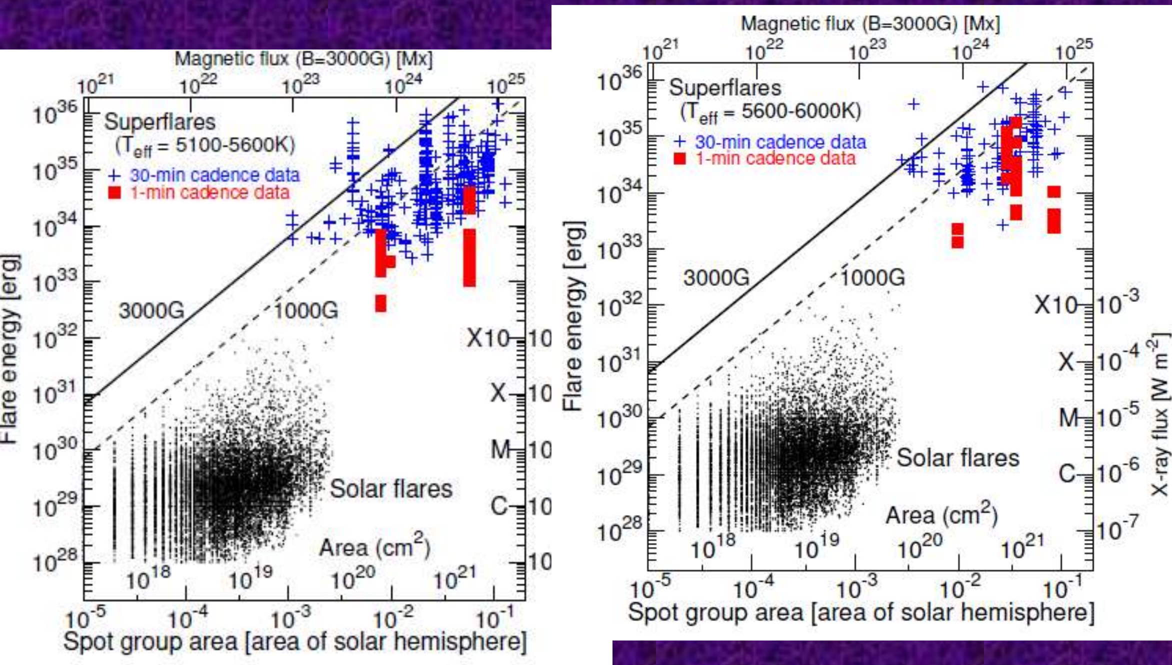

$$E_{\rm flare} \approx f E_{\rm mag} \approx f \frac{B^2 L^3}{8\pi} \approx f \frac{B^2}{8\pi} A_{\rm spot}^{3/2}$$

$$\approx 7 \times 10^{32} ({\rm erg}) \left(\frac{f}{0.1}\right) \left(\frac{B}{10^3 {\rm G}}\right)^2 \left(\frac{A_{\rm spot}}{3 \times 10^{19} {\rm cm}^2}\right)^{3/2}$$

$$\approx 7 \times 10^{32} ({\rm erg}) \left(\frac{f}{0.1}\right) \left(\frac{B}{10^3 {\rm G}}\right)^2 \left(\frac{A_{\rm spot}/(2\pi R_\odot^2)}{0.001}\right)^{3/2}$$

*** The mean value of the magnetic field |B| for Young Suns is around 5 G (Marsden et al. (2013) – "Bcool collaboration".

Superflares on G-type stars detected from short- (Maehara, 2015) and long-cadence data (Shibayama et al. 2013, Notsu et al. 2019) respectively.

The total flare energy E_{flare} Is a function of amplitude, mean magnetic field and inclination of rotation axis of a star to line of sight.

#The bolometric energy released by flares E_{flare} is almost consistent with the magnetic energy E_{mag} stored around the large star spots.

But the strongest flares do not always correlate with the largest starspot groups (Rottenbacher, Vida 2018).

E_{flare} , Spot Group Area A, & Flare Frequency vs P_{rot}

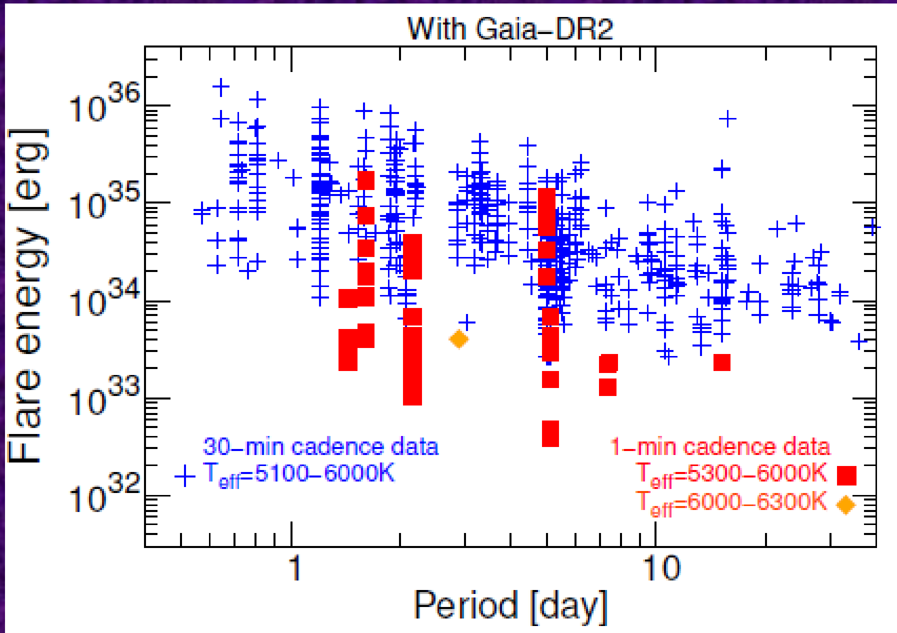

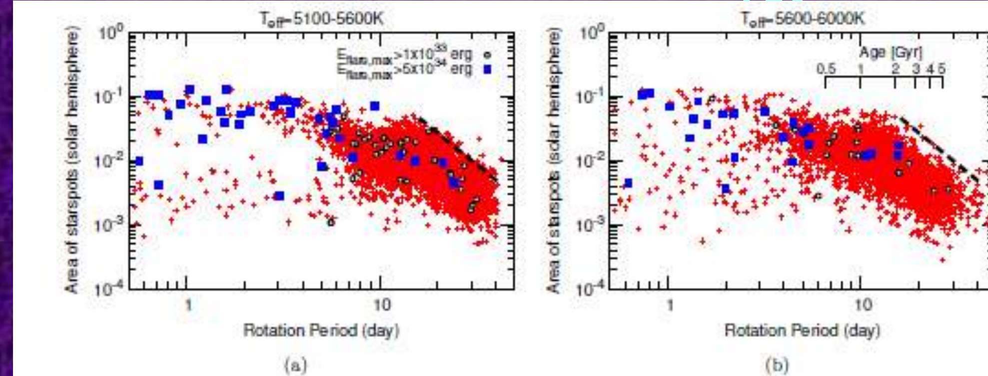

Figure 15. Scatter plot of the spot group area of solar-type stars (A_{spot}) as a function of the rotati period (P_{rot}), using the data updated with $T_{eff,DR25}$ and R_{Gaia} values in this study. The vertical ax represents A_{spot} in units of the area of solar hemisphere ($A_{1/2\odot} \sim 3 \times 10^{22}$ cm^2). Open circles and blue fille squares indicate solar-type stars that have superflares with the energy values of their most energetic flar $E_{flare,max} > 1 \times 10^{33}$ erg and $E_{flare,max} > 5 \times 10^{34}$ erg, respectively. Red small cross marks indicate solar-ty stars without superflares. The plotted data are separated into (a) and (b) on the basis of the temperatu values: **(a)** T_{eff} = 5100 – 5600 K and **(b)** T_{eff} = 5600 – 6000 K. The black dashed line in (a) is plotted b eye to roughly show the upper limit of the datapoints in the range of $P_{rot} \gtrsim 14$ days. The black dashed li in (b) is plotted at the same place as (a) in order for comparison with the results of (a). Only in (b), w also added the scale of stellar age (t) on the basis of the gyrochronology relation of solar-type star ($t \propto P^{0}_{ro}$ Ayres 1997) (See the main text of Section 5.3 for the details).

Notsu et al. arXiv 2 Apr 2019, 1904.00142

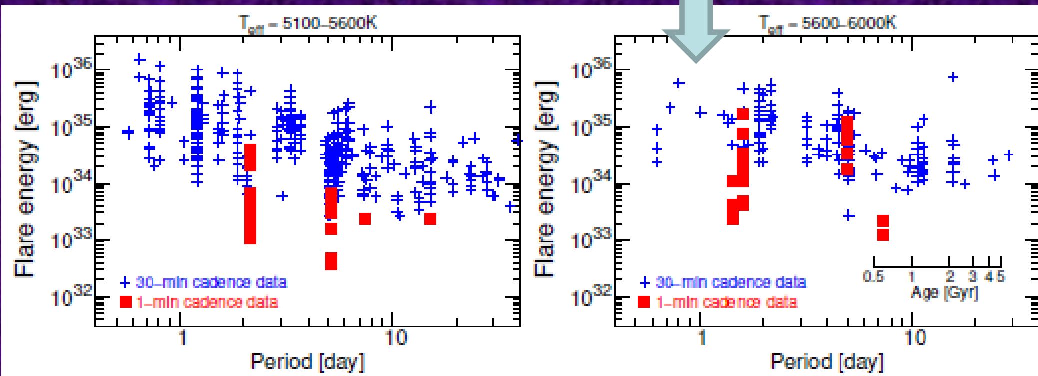

Rotation period, day

(b)

Figure 13. Scatter plot of the superflare energy (E_{flare}) vs. the rotation period (P_{rot}) of each star (as Figure 12(b)). Blue plus marks and red filled squares are the data of superflares found from *Kepler* 30-min and 1-min time cadence data, which are originally in Figure 12(b). They are separated into (a) and (b) on the basis of the stellar temperature values: **(a)** T_{eff} = 5100 – 5600 K and **(b)** T_{eff} = 5600 – 6000 K. Only in (b), we added the scale of stellar age (t) on the basis of the gyrochronology relation of solar-type star ($t \propto P^{0.6}_{rot}$: Ayres 1997) (See main text for the details).

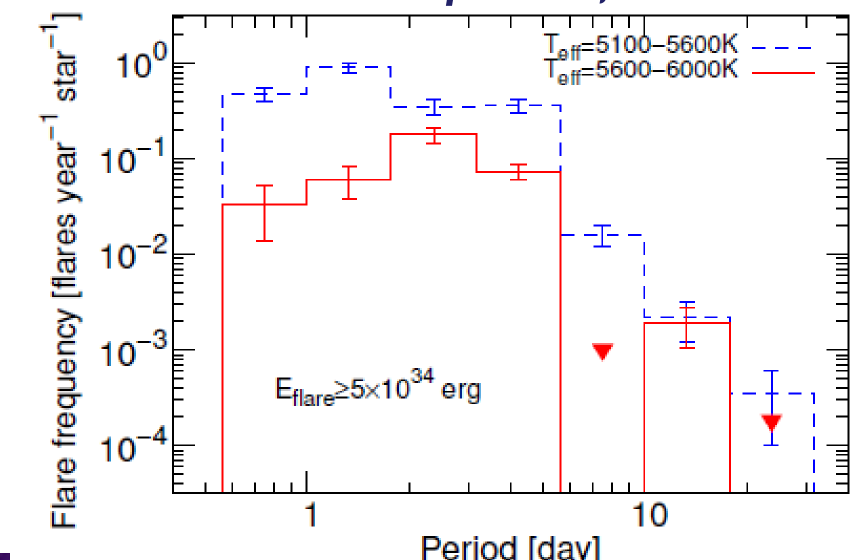

Flare Occurrence Frequency on G-Type Stars

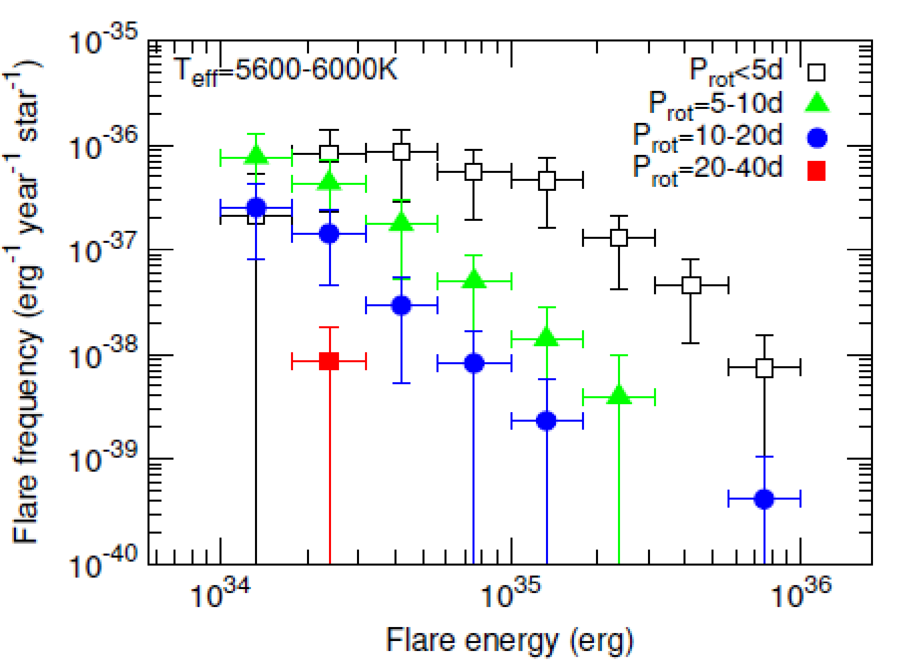

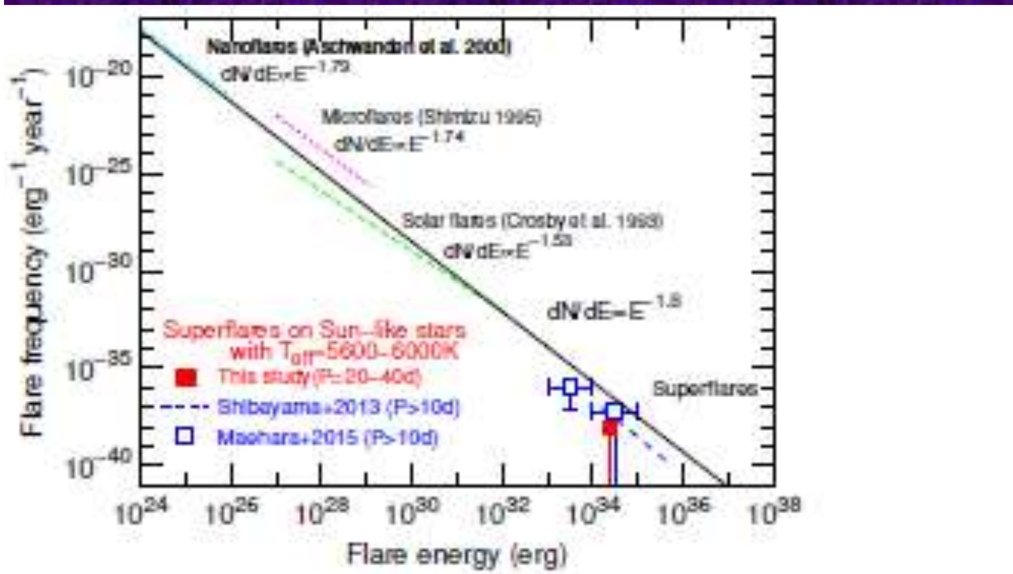

Figure 17. The comparison between the frequency distribution of superflares and solar flares. The red square, blue dashed line, and blue open squares indicate the occurrence frequency distributions of superflares on Sun-like stars (slowly-rotating solar-type stars with T_{eff} = 5600 − 6000 K). The red square corresponds to the updated frequency value of superflares on the stars with P_{rot} = 20 − 40 days, which are calculated in this study and presented in Figure 16. Horizontal and vertical error bars are the same as those in Figure 16. For reference, the blue dashed line and blue open squares are the values of superflares on the stars with P_{rot} >10 days, which we presented in Figure 4 of Maehara et al. (2015) on the basis of original superflare data using *Kepler* 30-min cadence data (Shibayama et al. 2013) and 1-min cadence data (Maehara et al. 2015), respectively. Definitions of error bars of the blue open squares are the same as those in Figure 4 of Maehara et al. (2015). Three dashed lines in upper-left side of this figure indicate the power-law frequency distribution of solar flares observed in hard X-ray (Crosby et al. 1993), soft X-ray (Shimizu 1995), and EUV (Aschwanden et al. 2000). Occurrence frequency distributions of superflares on Sun-like stars and solar flares are roughly on the same power-law line with an index of −1.8 (black solid line) for the wide energy range between 10^{24} and 10^{35} erg.

P_{rot} < 5 d   Age t < 0.5 Gyr

P_{rot} = 5-10 d   t = 0.5 -1 Gyr

P_{rot}=10 -20d   t = 1-3.2 Gyr

P_{rot}=20-40 d   t > 3.2 Gyr

Notsu et al. arXiv 2 Apr 2019, 1904.00142

Statistics of Kepler' s Superflares

Maehara et al. 2015 : 1547 single solar-like stars with 5300 K < T_{eff} < 6300 K and 4.0 < log g< 4.8.

187 flares with the total energy from 2×10^{32} erg to 8×10^{35} erg were registered in the only 23 such stars

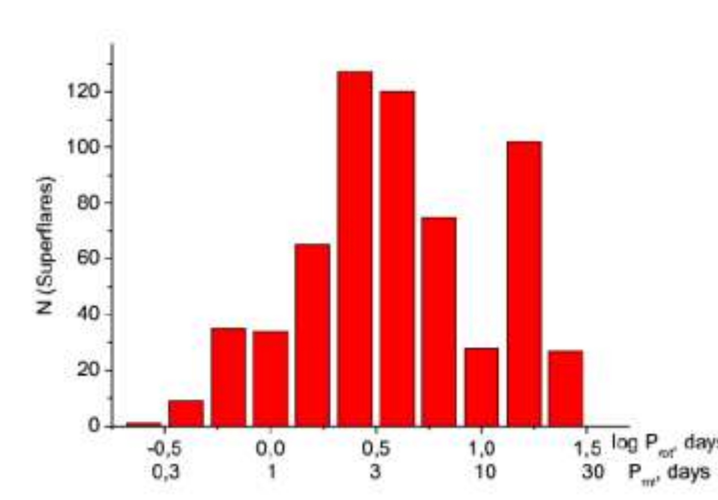

 # The mean flare occurrence frequency for events with the total energy

10^{33} erg – one event per 70-100 yrs,

10^{34} erg – occurs once in about 500-800 yrs

10^{35} erg – once in about 4000-5000 yrs

The average rate of appearance of an X100 class flare on a G-star with P_{rot} = 25 d (like the Sun) is one event in 500-600 years

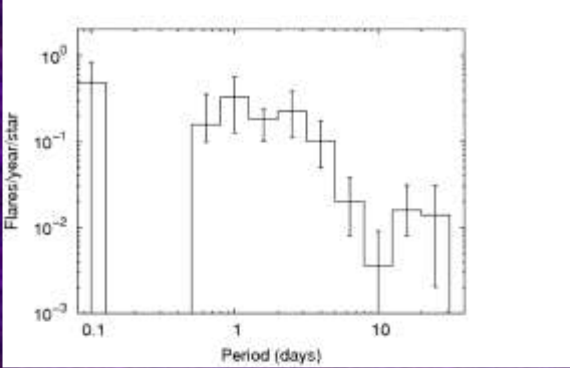

Only 0.2 to 0.3% of solar-type stars show superflares

On the origin of superflares on G-type stars of different ages and their maximum energy : Katsova & Livshits 2015 Solar Phys. V. 290

Where the Kepler Mission Registered Flares with $E_{tot} > 10^{35}$ erg ?

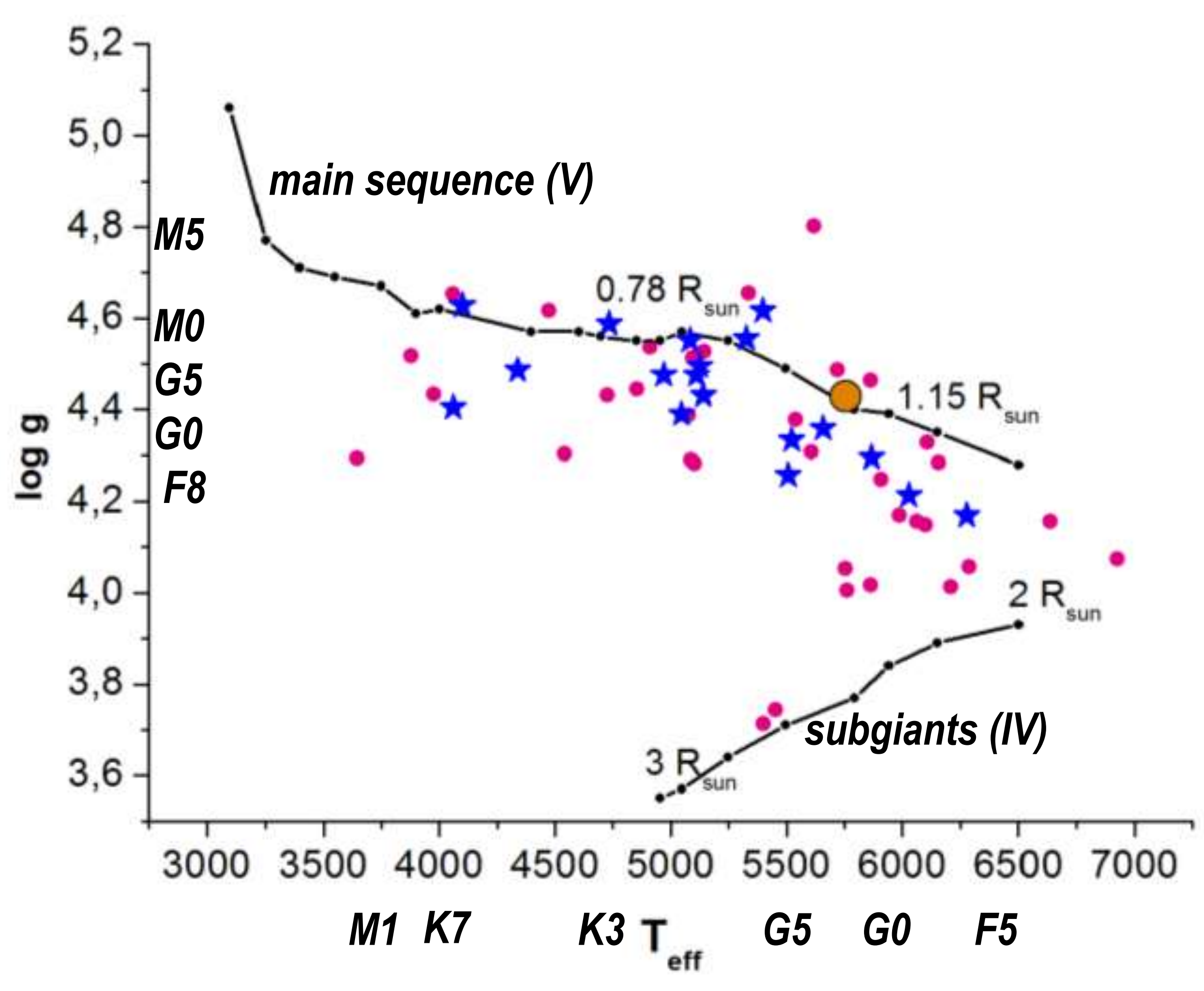

F and G subgiants (incl components of close binaries)

Blue asterisks :

Eclipsing binaries :

EA - detaches

EB – semi-detaches

Red circles :

Single solar-type stars

(Katsova & Nizamov, G & A 2018)

Lines correspond to Fundamental stellar parameters derived from the evolutionary tracks" by Straizys, Kuriliene, 1981

Conclusions from the Kepler Mission

(i) More than 40% of the original solar-type superflare stars in the previous studies are now classied as subgiants .

(i) The bolometric energy released by flares, E_{flare} , is consistent with the magnetic energy (E_{mag}) stored around the large star spots .

(iii) The maximum superflare energy, E_{flare}, continuously decreases as the P_{rot} increases (as the star becomes older).

Superflares up to 10^{36} erg can occur on young rapidly-rotating stars (P_{rot} ~ a few days and t ~ a few hundreds Myr), and the flare frequency of such young stars is 100 times higher as compared with the old slowly-rotating Sun-like stars.
In contrast, Superflares with E = 5 x10^{34} erg occur on old, slowly-rotating Sun-like stars (T_e = 5600 - 6000 K, P_{rot} = 25 days, and age t = 4.6 Gyr) approximately once every 2000 - 3000 years. The upper limit of starspot size values on these stars would be ~ a few ×10^{-2} $A_{1/2\odot}$ (Notsu et al. 2019)

The solar-type stars with large amplitude photometric variations (1 %) have large starspots with the area of the order of $10^{-2}A_{1/2\odot}$ and the lifetime of such large spots ranges from 50 - 300 days which is longer enough than P_{rot} of the star. (Namekata et al. arXiv Nov 2018)

iv) The maximum area of starspots , A, does not depend on P_{rot} and are roughly constant or very gentle decreasing trend around $A_{spot} = 5\times10^{-2} - 1\times10^{-1} A_{1/2\,\odot}$ ($A_{1/2\,\odot} \sim 3\times10^{22}$ cm^2 $\odot$-hemisphere) when the star is young and rapidly-rotating.

However, as the star becomes older and its rotation slows down, it starts to have a steep decreasing trend at a certain period: $P_{rot} \sim 12$ days ($t \sim 1.4$ Gyr) for the stars with $T_e = 5600 - 6000$ K , and $P_{rot} \sim 14$ days for the stars with $T_e = 5100 - 5600$ K. Maximum size of starspots on slowly-rotating Sun-like stars is 1 % of the solar hemisphere, and this is enough for generating superflares with the $E_{flare} \leq 5\times10^{34}$ erg.

v) These decreasing trends of the maximum E_{flare} and the maximum A can be related with each other since the superflare energy can be explained by the starspot magnetic energy. However, there is also a difference between the two: the maximum A starts to steeply decrease at a certain P_{rot} , while the maximum E_{flare} continuously decrease as the rotation slows down This can suggest a possibility that the E_{flare} is determined not only by the A, but also by other important factors (e.g., spot magnetic structure).

Notsu et al., 2019

What can confirm the solar-type mechanism for stellar superflares ?

- The hard X-rays in stellar flares -- till now the sensitivity is not enough
- Microwave bursts at the maximum of the flare on a star at 100 pc :

For a large solar flare, the total injection is $N = 10^{36}$ electrons/s .

- For a stellar flare with $F = 3{\times}10^{11}$ erg/cm^2 s and $S_{opt} = 4 \times 10^{18}$ cm^2, this total number of these accelerated electrons is $N = 10^{38}$ per s.

The microwave flux of such a superflare on the star at the distance of 100 pc is estimated as 2 mJy. Under favourable conditions such a microwave flux can be detected.

(Katsova & Livshits 2015, Solar Phys. V.290 P.3663)

- The Lithium production by spallation reactions during stellar flares :

The appearance of a large amount of Li and its diffusion over the surface during some big solar flares –

- The theoretical estimate by M. Livshits, Sol. Phys. 173/2, 377 (1997);
- Observations: # 4B Solar Flare of 9 March 1989 by W.Livingston et al. (1997);

Li I line enhancement during the big flare on a late-type star by D. Montes, L.W. Ramsey, A & A, 340, L5 (1998), see also Ramaty et al. ApJ. (2000)

Flares on the Young Sun and Today

- Kappa[1] Cet (G5 V) P_{rot} = 9.4 d, $L_x = 10^{29}$ erg/s
- Flare Frequency Occurrence with $E > 10^{32}$ erg
  - 5 events / day → 1825 events / year

    (from EUVE data – M. Audard et al. 2000, ApJ)

- The Young Sun: spot area: 10–20 times larger
- Large-scale magnetic field : 10–15 times stronger
- Superflares: the total flare energy $E \leq 5 \times 10^{34}$ erg

  The contemporary Sun:

  1144 proton flares ($E \geq 10$ MeV) during 1975 – 2003

  = 41 events / year (Belov et al. 2005)

Even the largest ARs on the contemporary Sun are capable of producing non-stationary processes (flares and CME) with total energy not greater than 3×10^{32} erg (Katsova , Livshits 2015; Katsova et al .2018)

Conclusions and Some Meaning – I

- *Initial conditions in a protostar when it arrives on the main sequence rule a scenario of further evolution of its activity.*

  The stellar mass determines a depth of the convection zone. Relationship between chromospheric and coronal activity levels depends on the depth of the convection zone, i.e. it is changed vs spectral class.
- *The saturated regime of activity at earlier epochs of evolution changes to the solar-type activity and it occurs at various rotation periods for G, K and M stars.*
- *Most of Superflares occur rather at this epoch of the saturated regime of activity.*
-

2 –

Conclusions – II

Flares stronger than 3×10^{32} erg can not occur on the contemporary Sun (Katsova & Livshits 2015; Katsova et al. 2018).

Observations of magnetic fields on young main-sequence G-type stars (with $P_{rot} \sim 8 - 10$ d and Age ~1 Gyr) determine that the maximal E_{flare} there can not exceed 5×10^{34} erg.

For such events only, we can conclude that their origin is similar to solar one: when deposit of the free energy occurs in the chromosphere and then it is realized during a non-stationary process.

Therefore, for explanation the more powerful phenomena with $E \geq 10^{35}$ erg we should attract other sources of the energy or another dynamo regime …

(Katsova & Livshits 2015; Katsova et al. 2018a; 2018b).

Be careful working with the Sun and Thanks for your attention